AD-A100 492 VOUGHT CORP ADVANCED TECHNOLOGY CENTER DALLAS TX F/G 11/4
THE EFFECT OF ENVIRONMENT ON THE MECHANICAL BEHAVIOR OF AS/3501--ETC(U)
JAN 81 T HO, R A SCHAPERY N00019-79-C-0580
UNCLASSIFIED ATC-R-92100/ICR-5 NL

END
DATE FILMED
7-81
DTIC

UNCLASSIFIED

SECURITY CLASSIFICATION OF THIS PAGE (When Data Entered)

REPORT DOCUMENTATION PAGE	READ INSTRUCTIONS BEFORE COMPLETING FORM
1. REPORT NUMBER	2. GOVT ACCESSION NO. AD 100492 / 3. RECIPIENT'S CATALOG NUMBER
4. TITLE (and Subtitle) The Effect of Environment on the Mechanical Behavior of AS/3501-6 Graphite/Epoxy Material Phase III	5. TYPE OF REPORT & PERIOD COVERED Final Report for Period 1 Sept 1979 - 31 Oct 1980
	6. PERFORMING ORG. REPORT NUMBER R-92100/1CR-5 ✓
7. AUTHOR(s) T. Ho R. A. Schapery	8. CONTRACT OR GRANT NUMBER(s) N00019-79-C-0580
9. PERFORMING ORGANIZATION NAME AND ADDRESS Vought Corporation Advanced Technology Center P. O. Box 226144 Dallas, Texas 75222	10. PROGRAM ELEMENT, PROJECT, TASK AREA & WORK UNIT NUMBERS --
11. CONTROLLING OFFICE NAME AND ADDRESS Department of the Navy Naval Air Systems Command Washington, D.C. 20361 Code AIR 52032D	12. REPORT DATE January 1981
	13. NUMBER OF PAGES 70
14. MONITORING AGENCY NAME & ADDRESS(if different from Controlling Office) --	15. SECURITY CLASS. (of this report) Unclassified
	15a. DECLASSIFICATION/DOWNGRADING SCHEDULE --

16. DISTRIBUTION STATEMENT (of this Report)

Approved for public release; distribution unlimited

17. DISTRIBUTION STATEMENT (of the abstract entered in Block 20, if different from Report)

18. SUPPLEMENTARY NOTES

19. KEY WORDS (Continue on reverse side if necessary and identify by block number)

Composite, Temperature, Humidity, Fatigue, Matrix Modulus

20. ABSTRACT (Continue on reverse side if necessary and identify by block number)

The effect of temperature and moisture on the fatigue properties of AS/3501-6 Gr/Ep composite was investigated. The test specimens used were of layup $(\pm 45/90_2)_s$ and $(0/\pm 45/90)_s$. Constant stress amplitude fatigue tests of these specimens and their data analysis were conducted. A probabilistic fatigue failure model derived from the concept of crack propagation has been used as a base for data/analysis correlation. Current data show that the degraded effective modulus of the in-situ matrix should be an important parameter in the analysis of fatigue life prediction.

DD FORM 1 JAN 73 1473 EDITION OF 1 NOV 65 IS OBSOLETE S/N 0102-LF-014-6601

UNCLASSIFIED

SECURITY CLASSIFICATION OF THIS PAGE (When Data Entered)

the analysis of fatigue life prediction.

FORWARD

This technical report is for Phase III of the program entitled "The Effect of Environment on the Mechanical Behavior of AS/3501-6 Graphite/Epoxy Material". The work was performed at Vought Corporation Advanced Technology Center. The program is sponsored by the Naval Air Systems Command under Contract N00019-79-C-0580.

Mr. M. Stander is the Navy Project Manager and Dr. W. J. Renton is the Vought Program Manager. Technical personnel involved are Dr. T. Ho, Principal Investigator, and Dr. R. A. Schapery, Texas A&M University, Technical Consultant.

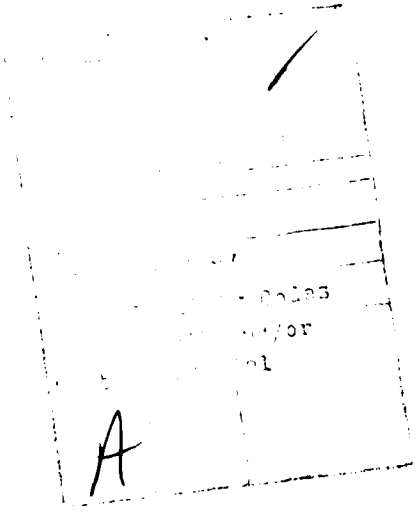

TABLE OF CONTENTS

LIST OF FIGURES

LIST OF FIGURES (Cont'd)

LIST OF TABLES

1.0 INTRODUCTION

Wide usage of advanced composite materials in aerospace systems is expected to become a reality over the next few years. A V/STOL fighter aircraft is one of several Navy articles projected to be increasingly dependent on composite materials for primary and secondary structural components.

Presently, the response of advanced composite materials to arbitrary load and environments is not well-understood, and service conditions often have a significant adverse effect on the material's performance. Analysis of structural response to severe environments and related fatigue lifetime prediction methods is presently insufficient. This composites research program will assist in resolving this deficiency in the technology base. This in turn will ensure that the confident usage of advanced composite materials by the stress analyst and designer can be attained in the near future.

The overall objectives of this research program are:

- o To ascertain if the mechanical response of AS/3501-6 graphite/epoxy composite material, subject to various time, temperature and moisture effects, can be characterized using traditional viscoelastic shift factors, and to formulate a master curve of material property dependence on time, temperature and humidity.
- o To ascertain the feasibility of predicting fatigue failure of a composite material by accounting for the linear viscoelastic behavior of the resin in various temperature and humidity environments.
- o To determine if a specific thermal conditioning environment can be directly substituted for a specific moisture conditioning environment, over a prescribed temperature vs. humidity range for AS/3501-6 graphite/epoxy material, and obtain an equivalent moisture effect on mechanical

and fatigue properties. If this can be shown, a substantial cost and time savings in moisture conditioning of the test specimen can be achieved and possibly extended to other composite specimens.

During the first phase of this program[1], the basic quasi-static properties of AS/3501-6 graphite/epoxy composite material, subjected to various temperature and humidity environments, were characterized through linear viscoelastic theory. The first and third objectives were achieved, at least for the environments investigated. This Phase III program is a continuation of the Phase II[2] effort to investigate the fatigue characteristics of composites, which is the second objective of this research program. Analytical and experimental studies were conducted and the results obtained thus far are covered in this report. Specifically, fatigue tests for specimens of practical layups $(\pm 45/90_2)_s$ and $(0/\pm 45/90)_s$ were conducted at four temperature/humidity environments. Analysis indicates that the effective matrix modulus, as affected by fatigue damage and the environments, has an important bearing in the basic fatigue mechanism and the fatigue analysis model.

Test results in Phase II and Phase III will provide adequate amounts of data for the evaluation in Phase IV of the proposed basic fatigue failure mechanism.

2.0 SPECIMEN FABRICATION AND ENVIRONMENTAL CONDITIONING

Hercules AS/3501-6 prepreg tape was used to prepare the specimens for this program. Ten composite panels (Table 1) were fabricated by Vought's Manufacturing Research and Development Division per the fabrication procedure in Table 2 as recommended by Hercules. Panels A, B, and C were for twenty ply 90^{o} specimens and Panel D was for eight ply $\pm 45^{o}$ specimens. Panels E1, E2, and E3 were for quasi-isotropic layup $(0/\pm 45/90)_{S}$. Panels F1, F2 and F3 were of layup $(\pm 45/90_{2})_{S}$. Each panel was inspected with ultrasonic C-scan and defects were found only in panel A using photomicrographs.

A process control panel which is of unidirectional layup was separately made to evaluate the quality of the panels. The mechanical properties of the specimens from the process control panel are summarized in Table 3. The flexural strength, flexural modulus and short beam shear results indicate that our panels yield comparable properties with vendor published values for AS/3501-6 composite.

The fatigue specimens are 7.0" long by .75" wide as shown in Figure 1 which is suitable for the Shore Western test machine. A specimen fabrication procedure modified from Phase II to make fatigue specimens was used and is shown in Figure 2. This procedure minimizes edge defects resulting from conventional cutting techniques. Inspection of the specimen surface under the 16x microscope shows the wafering diamond cutter does produce a quality surface finish. Most machining defects are not large enough to see at 16X on the wafering cut surface, including the edge area.

TABLE 1. COMPOSITE PANELS FOR THE PROGRAM

PANEL ID	ORIENTATION	DIMENSION	C-SCAN RESULT	NO. OF SPECIMENS	PHOTOMICROGRAPH ON SPECIMENS
A, B	$(90)_{20}$	16" x 20" x 0.1"	No Defect	71	Showed High Porosity in A-Panel
C	$(90)_{20}$	16" x 14" x 0.1"	No Defect	25	OK
D	$(\pm 45)_{2S}$	16" x 14" x 0.04"	No Defect	28	OK
E_1, E_2	$(0/\pm 45/90)_S$	16" x 20" x 0.04"	No Defect	84	OK
E_3	$(0/\pm 45/90)_S$	16" x 14" x 0.04"	No Defect	36	OK
F_1, F_2	$(\pm 45/90_2)_S$	16" x 20" x 0.04"	No Defect	64	OK
F_3	$(\pm 45/90_2)_S$	8" x 15" x 0.04"	No Defect	16	OK

TABLE 2. THE LAYUP PROCEDURE AND CURE CYCLE FOR AS/3501-6

The layup procedure was:

- Clean all tooling
- Apply a mold release agent to the tooling and caul plate
- Cover both surfaces of the layup with TX-1040
- Position the layup on the tool
- Apply the cork dam and 6 bleeder plies
- Cover the layup with nylon film
- Cover the layup with two plies of fiberglass breather cloth
- Install the layup in a vacuum bag and place in an autoclave

The cure cycle was:

- Apply 25" Hg minimum vacuum
- Apply 10 psi autoclave pressure
- Heat to 350 $\pm$ 5°F (5-10°F/min rate)
- Apply 90 $\pm$ 5 psi autoclave pressure when the panel reaches 275 $\pm$ 5°F (DO NOT VENT)
- Maintain the laminate at 350 $\pm$ 5°F for 120 $\pm$ 5 minutes
- Cool slowly to below 150°F (Cool no faster than 5°F per minute - Cool down should take approximately 45 minutes)

TABLE 3. MECHANICAL PROPERTIES OF PROCESS CONTROL PANEL.

SHORT BEAM SHEAR (PSI)	FLEXURAL STRENGTH (PSI)	FLEXURAL MODULUS (10^6 PSI)
20,904	247,983	17.9
21,204	241,935	18.5
27,051	259,523	19.3
AVE. 20,719(17,500)	249,814(260,000)	18.6(20.6)

NOTE 1: Average Fiber Volume Content is 68.2% For The Panels

2: Vendor Data Are in Parentheses For a 62% Fiber Volume Per AS/3501-6 Data Sheet

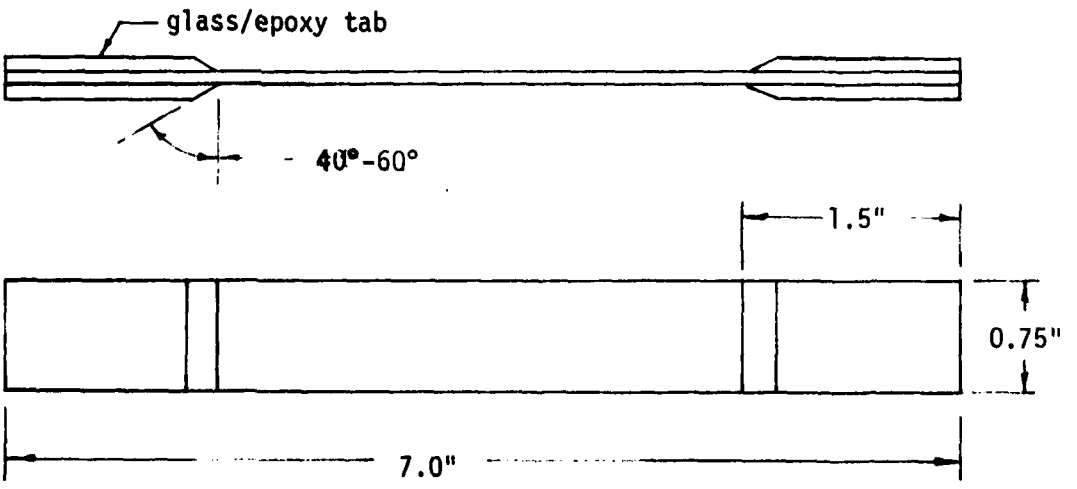

FIGURE 1. TYPICAL FATIGUE SPECIMEN.

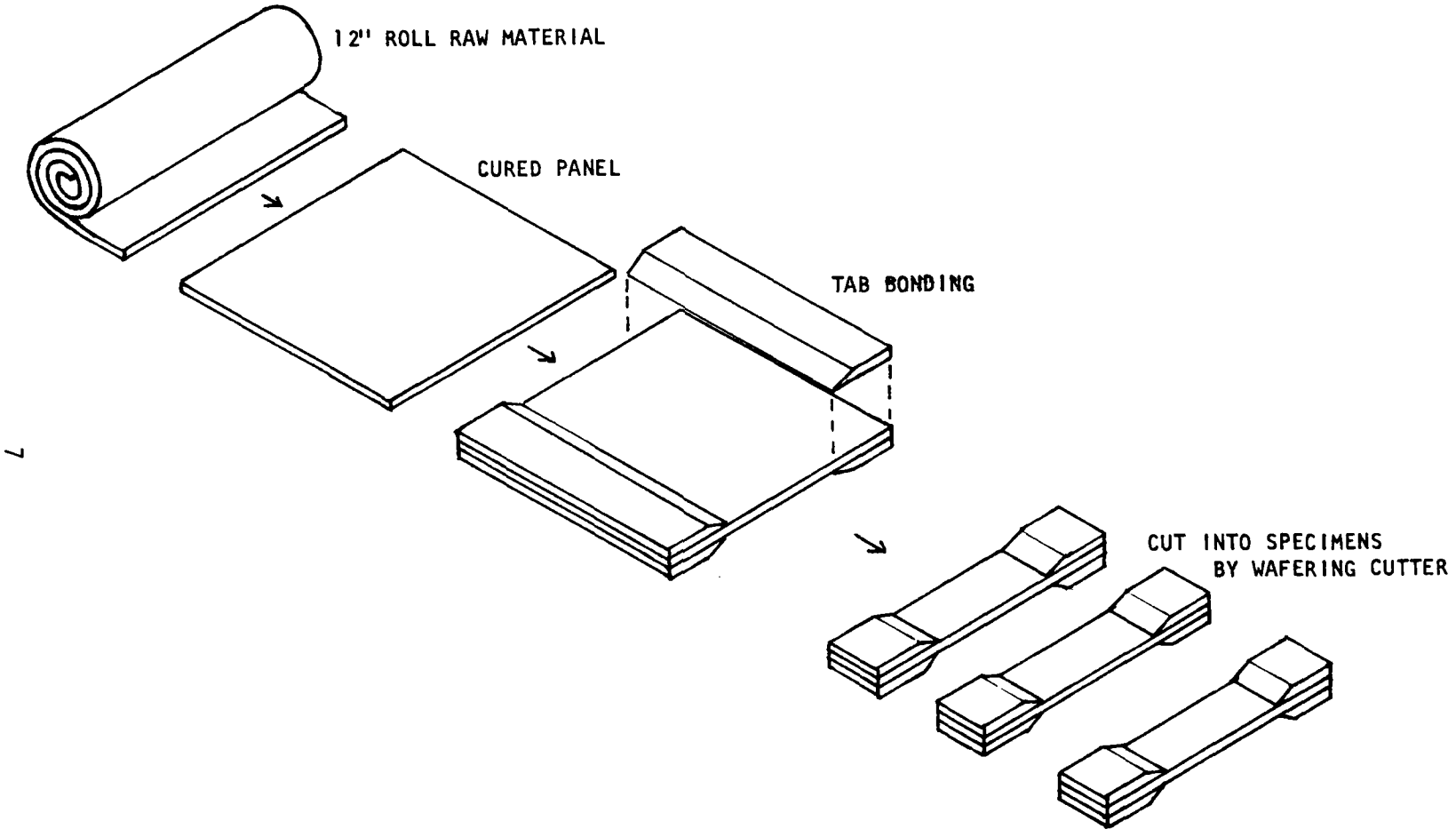

FIGURE 2. FATIGUE SPECIMEN FABRICATION PROCEDURE.

A total of 324 specimens were fabricated according to Table 1. In general, 90^{o} panels usually are of worse quality than that of other panels. Figure 3 indicates the typical bad areas observed on some 90^{o} specimen surfaces that were not detected by the C-scan technique. It seems that twenty plies of 90^{o} layers did trap some volatiles in the laminate during the curing process and created a porosity problem.

An enclosed glass chamber and a forced air oven were used to environmentally condition the specimens to the desired moisture level. A saturated aqueous solution of Sodium Bromide (NaBr) in contact with a solid phase of the salt at $170^{o}F$ temperature was used to generate the 50% relative humidity level and that of Sodium Fluoride (NaF) was used to generate the 95% relative humidity level. Based on results of Phase II, 85 days of conditioning are necessary to insure that the 90^{o} specimens with a 0.10" thickness attain at least 95% saturation at the $170^{o}F$ temperature environment, while fifteen days of conditioning are required for the other three types of specimen layups with 0.04" thickness.

Before environmentally conditioning the specimens, tab areas of all the specimens except for Panel E3 were coated with Ecco-coat VE on top of scotch tape to slow down the ingress of moisture into the bondline so that the shear strength of the adhesive in the tab area could be maintained at the desired level (around 5000 psi adhesive shear strength at room temperature) during the fatigue test. Specimens from Panel E3 were wrapped with aluminum backing tape instead of scotch tape. Fatigue test results for $(0/\pm 45/90)_{s}$ specimens indicated that only minor improvement in resisting moisture was produced by using the aluminum backing tape.

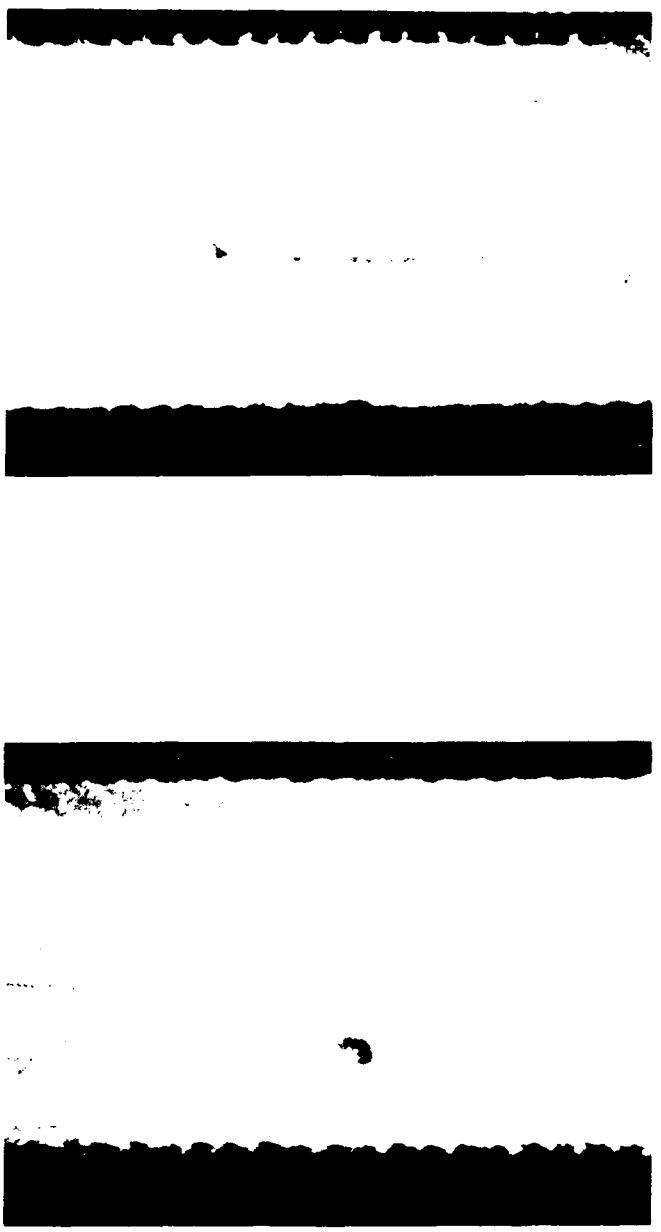

FIGURE 3. POROSITY OBSERVED ON THE EDGE OF 90°-SPECIMENS. (16x)

3.0 TEST PROCEDURE

Static and fatigue tests were conducted according to the test matrix in Table 4. Static tests provide data to evaluate the batch to batch property variations and to characterize the basic material properties. Static load-displacement relations at various environments were recorded on both a strip chart recorder and X-Y plotter. Fatigue tests were conducted within various constant environments by keeping the mean stress level, stress amplitude, and environment unchanged during the fatigue cycling.

The general static and fatigue test arrangement is shown in Figure 4. Two environmental extensometers[1] were used to monitor the displacements during the static tests and fatigue tests. Both extensometers were calibrated for environmental stability and accuracy at the beginning of the program. During the tests, each specimen also had a resistor type temperature sensor (ETG-50B from Micromeasurement) attached to its side surface. The load, LVDT readings, and temperature were recorded using a Sanborn strip chart recorder. The Shore Western test machine had a recording chart to monitor the temperature and humidity during the testing.

TABLE 4. TEST MATRIX

TEST	TYPE OF TEST	TEST ENVIRONMENT (°F/% R.H.)	REPLICAS PER ENVIRONMENT	NUMBER OF SPECIMENS			
				$(\pm 45)_{2s}$	$(90)_{20}$	$(0/\pm 45/90)_{s}$	$(\pm 45/90_2)_{s}$
A	Static	75/50	2			2	2
		100/50			2		
		100/95			2		
		132/50				2	2
		132/95				2	2
		150/50			2		
		150/95			2		
		170/50				2	2
B	Fatigue at Constant Stress Amplitude	75/50	3 Stress x 6			18	18
		100/50			18		
		100/95			18		
		132/50				18	18
		132/95				18	18
		150/50			18		
		150/95			18		
		170/50				18	18

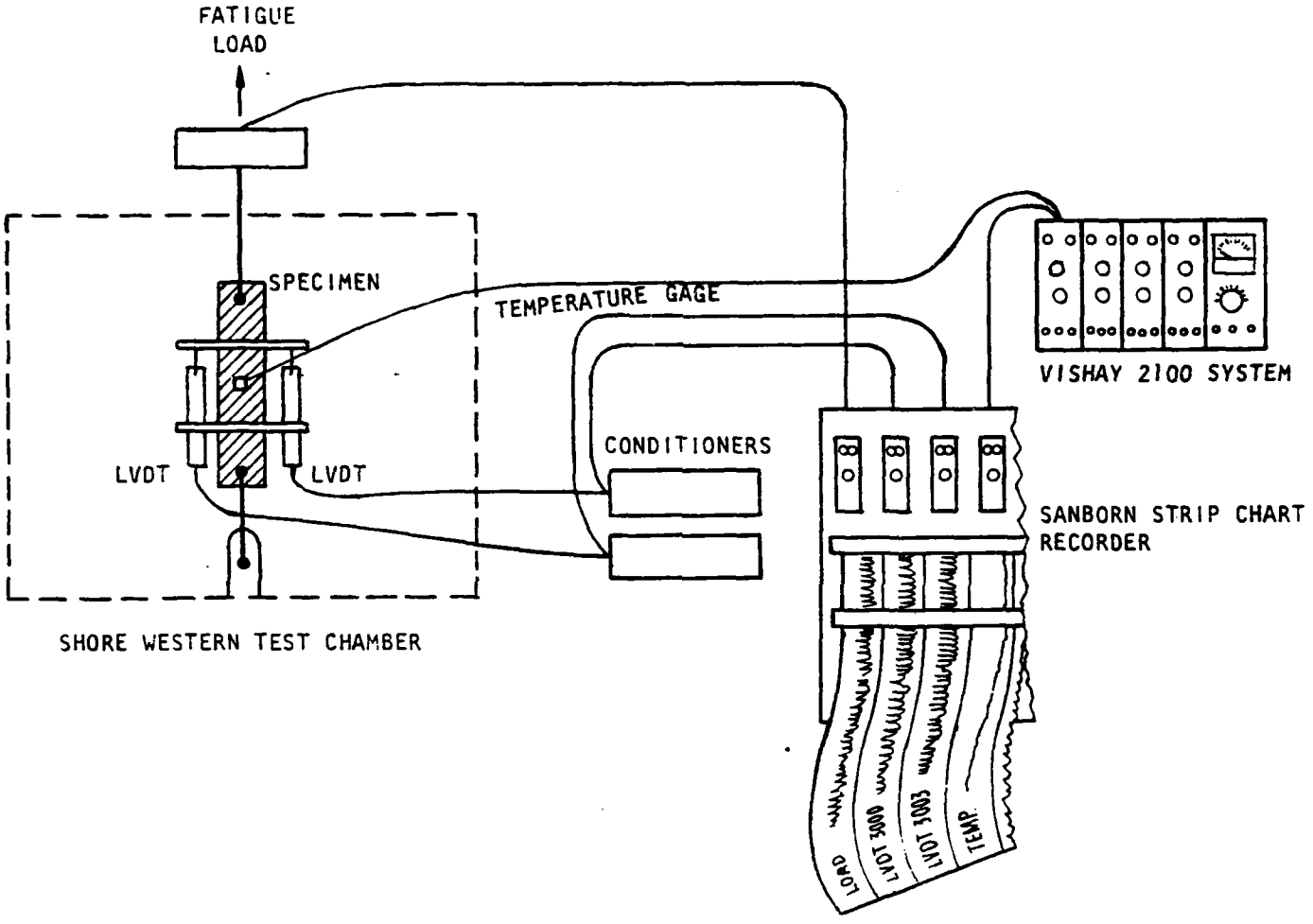

FIGURE 4. FATIGUE TEST ARRANGEMENT AND DATA ACQUISITION SYSTEM

4.0 STATIC TESTS AND ANALYSIS

All static specimens were conditioned to close to 95% of the saturated moisture levels in the environmental chamber before they were tested in their appropriate environments. The load rate was set at 250 lb/min. The four environments for specimens of layups $(0/\pm45/90)_2$ and $(\pm45/90_2)_s$ were 75°F/50%RH, 132°F/50%RH, 132°F/95%RH, and 170°F/50%RH. These were the environments used in Phase II for 90° specimens and $(\pm45)_{2s}$ specimens. The environments for 90° specimens in Phase III were 100°F/50%RH, 100°F/95%RH, 150°F/50% RH, and 150°F/95%RH and these environments are complementary to the previously mentioned four environments that were used in Phase II in order to broaden the data base for analysis.

The typical stress-strain curves for these three types of specimens are shown in Figure 5. The test results are shown in Table 5 for 90° specimens and Table 6 for specimen types $(0/\pm45/90)_s$ and $(\pm45/90_2)_s$. The 90° specimen data obtained from Phase II is also included in Table 5 for comparison. It is observed that the mechanical properties from the current batch is superior to that from the Phase II batch. One explanation for that difference, based on the experience with Kevlar/5208 system[3], is that the larger and thicker panels trap more volatile material in the laminate during the curing process. Panel sizes of 20" x 16" and 48" x 16" were used in Phase II. Smaller panels (20" x 16" or less) were fabricated in this Phase III program. This observation is also useful in explaining the fatigue characteristics of the 90° specimens.

Specimens of layup $(\pm45/90_2)_s$ have unique characteristics in their stress-strain behavior. A typical stress-strain curve is shown in Figure 6 and three characteristic regions common to all curves were observed. There are two distinct slope changes along each curve that are identified in Figure 6.

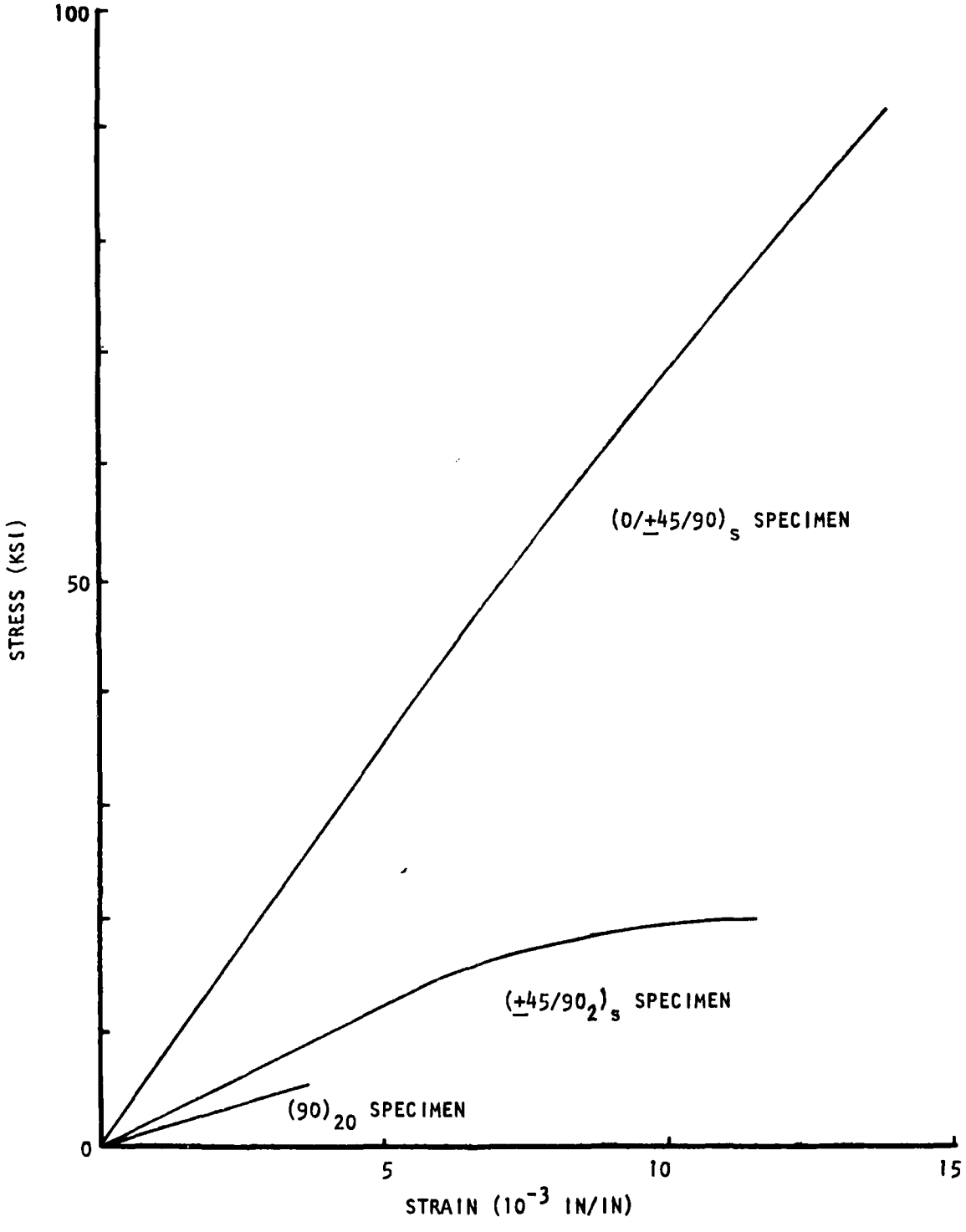

FIGURE 5. REPRESENTATIVE STRESS-STRAIN CURVES

TABLE 5. STATIC PROPERTIES OF 90°-SPECIMENS IN VARIOUS ENVIRONMENTS

	SPECIMEN ID	TEST ENVIRONMENT TEMP. (°F)	TEST ENVIRONMENT HUMIDITY (% R.H.)	ULTIMATE STRENGTH (KSI)	ULTIMATE STRAIN (μin/in)	YOUNG'S MODULUS (MSI)	FAILURE MODE EDGE +	FAILURE MODE GAGE *	FAILURE MODE HOLE
PHASE II	90-B4-1	75	As Fab.	7.41	4862	1.61	X		
	90-B8-8	75	As Fab.	6.52	4373	1.54	X		
	90-B1-4	75	50	4.58	3142	1.47	X		
	90-A4-1	75	95	4.16	3060	1.43		X	
	90-A4-2	75	95	3.76	2852	1.37		X	
	90-B3-6	132	50	4.83	3450	1.39	X		
	90-B3-7	132	50	4.73	3470	1.36		X	
	90-A17-3	132	95	2.64	2030	1.29	X		
	90-A17-4	132	95	3.46	2640	1.31	X		
	90-A4-3	132	95	3.89	3042	1.27	X		
	90-B3-4	170	50	5.00	3820	1.31		X	
	90-B3-5	170	50	5.65	4200	1.35		X	
	90-A17-1	170	95	3.08	2630	1.28		X	
	90-A17-2	170	95	3.86	3160	1.30	X		
PHASE III	A2-11	100	50	5.28	3630	1.453		X	
	A2-12	100	50	5.25	3720	1.411		X	
	C1-5	100	95	5.58	4084	1.366		X	
	C1-4	100	95	5.34	3901	1.369	X		
	C1-8	150	50	5.92	4129	1.434		X	
	A2-13	150	50	5.09	3666	1.390		X	
	A2-4	150	95	4.15	3104	1.338		X	
	C1-6	150	95	5.84	4338	1.347		X	

+ Edge: Failure location is in the tab end or end of middle gage section

* Gage: Failure location is in the gage section of the specimen

TABLE 6. STATIC PROPERTIES OF $(0/\pm45/90)_s$ SPECIMENS AND $(\pm45/90_2)_s$ SPECIMENS AT VARIOUS ENVIRNOMENTS

SPECIMEN LAYUP	SPECIMEN I.D.	TEST ENVIRONMENT		ULTIMATE LOAD (LBS)	ULTIMATE STRENGTH (PSI)	ULTIMATE STRAIN (μ in/in)	YOUNG'S MODULUS (MSI)	FAILURE MODE		
		TEMP (^{o}F)	HUMIDITY (% R.H.)					EDGE	GAGE	HOLE
$(0/\pm45/90)_s$	E1A7	75	50	3035	91970	13843	7.065		X	
	E1A6	75	50	2935	89177	13277	7.198		X	
	E1B15	132	50	2675	79566	12276	7.038		X	
	E1B14	132	50	2725	81174	11928	7.253		X	
	E1A10	132	95	2450	74536	12624	7.198	X		
	E1A9	132	95	2710	82221	12015	7.213		X	
	E1B3	170	50	2765	82023	12537	7.087		X	
	E1A8	170	50	2780	84576	13060	7.024			X
$(\pm45/90_2)_s$	F1A1-5	75	50	663	19761	10937	2.824		X	
	F1A1-6	75	50	658	19612	10150	2.735		X	
	F2A1-6	132	50	695	20472	10448	2.789		X	
	F2A1-5	132	50	694	20132	10448	2.794		X	
	F1A2-2	132	95	578	17203	11231	2.607		X	
	F1A2-1	132	95	558	16674	11405	2.559		X	
	F1A1-7	170	50	598	17823	11476	2.692		X	
	F1A1-8	170	50	600	17778	10357	2.633		X	

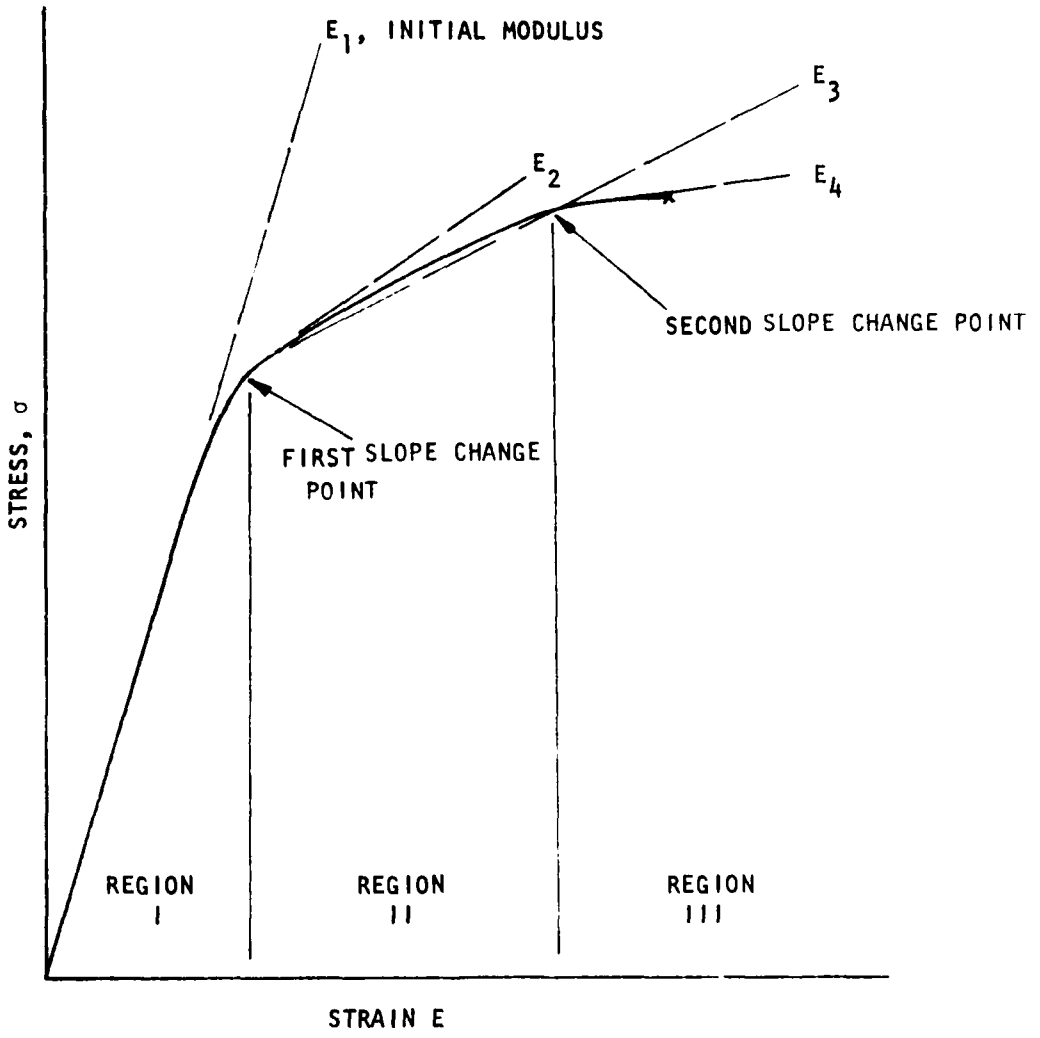

FIGURE 6 STRESS-STRAIN CURVE FOR $(\pm 45/90_2)_s$ TYPE SPECIMENS

The strain region between the initial point and the first slope change is designated as Region I. That between the first and second distinct slope change is designated as Region II. That between the second and the failure point is designated as Region III. Apparently the first slope change occurs when transverse cracking starts in the 90^{o} layers. The cracking action continues in Region II and the second slope change point is reached. The curve in Region III is relatively flat where the failure process accelerates. Mechanical response data related to these observations are summarized in Table 7 and normalized in Figure 7. The E_2 and E_3 values in Table 7 are the initial modulus and average modulus for Region II, respectively. The E_4 value is the initial modulus of Region III where 90^{o} lamina presumably do not support the axial load and provide only lateral constraint on the $\pm 45^{o}$ laminae. Two features of $(\pm 45/90_2)_s$ specimens that relate the static test results to a fatigue analysis can be summarized as follows:

a. The 90^{o} plies contribute to the laminate strength if the fatigue stress level is under 65% of the static ultimate strength. (Fig. 7)

b. As the fatigue loading continues, the $(\pm 45/90_2)_s$ specimen will creep under the mean stress and eventually fail in strain Regions II or III of Figure 6, with the 90^{o} lamina having only a few or many transverse cracks, respectively.

Static tests on $(0/\pm 45/90)_s$ specimens, which represent one type of common layup in structural applications, were also conducted to establish the baseline data for the fatigue tests. The results are shown in Table 8 and Figure 8. The environments seem to have little influence on the static properties of this quasi-isotropic laminate based on the results in Table 6.

TABLE 7. SLOPE CHANGE POINTS OF $(\pm 45/90_2)_s$ STRESS-STRAIN CURVES

ENVIRONMENT (°F/% RH)	SPECIMEN ID	FIRST SLOPE CHANGE POINT		SECOND SLOPE CHANGE POINT		MODULI (MSI)			
		STRESS (psi)	STRAIN (μ in/in)	STRESS (psi)	STRAIN (μ in/in)	E_1	E_2	E_3	E_4
75/50	F1A1-5	16,480	6,960	19,687	9,529	2.824	1.593	1.248	0.215
	F1A1-6	15,660	6,463	19,612	10,150	2.735	1.378	1.072	0.551
75/95	F1A1-2	11,899	4,391	18,221	9,694	2.706	1.443	1.192	0.687
	F1A1-1	12,422	4,640	18,133	9,694	2.622	1.337	1.130	0.588
132/50	F2A1-6	16,898	6.214	21,006	9,280	2.789	1.388	1.340	1.128
	F2A1-5	16,419	6,214	21,001	9,446	2.794	1.438	1.418	0.776
132/95	F1A2-2	12,213	4,806	16,831	9,114	2.607	1,359	1.072	0.301
	F1A2-1	12,562	5,137	15,926	8,369	2.559	1.123	1.041	0.181
170/50	F1A1-7	12,752	4,889	17,524	8,949	2.692	1.464	1.175	0.293
	F1A1-8	12,444	4,889	17,111	8,700	2.633	1.284	1.225	0.291
170/95	F1A1-3	12,735	5.220	15,118	7,209	2.530	1.394	1.198	0.430
	F1A1-4	12,230	4,889	15,660	8,286	2.552	1.378	1.010	0.379

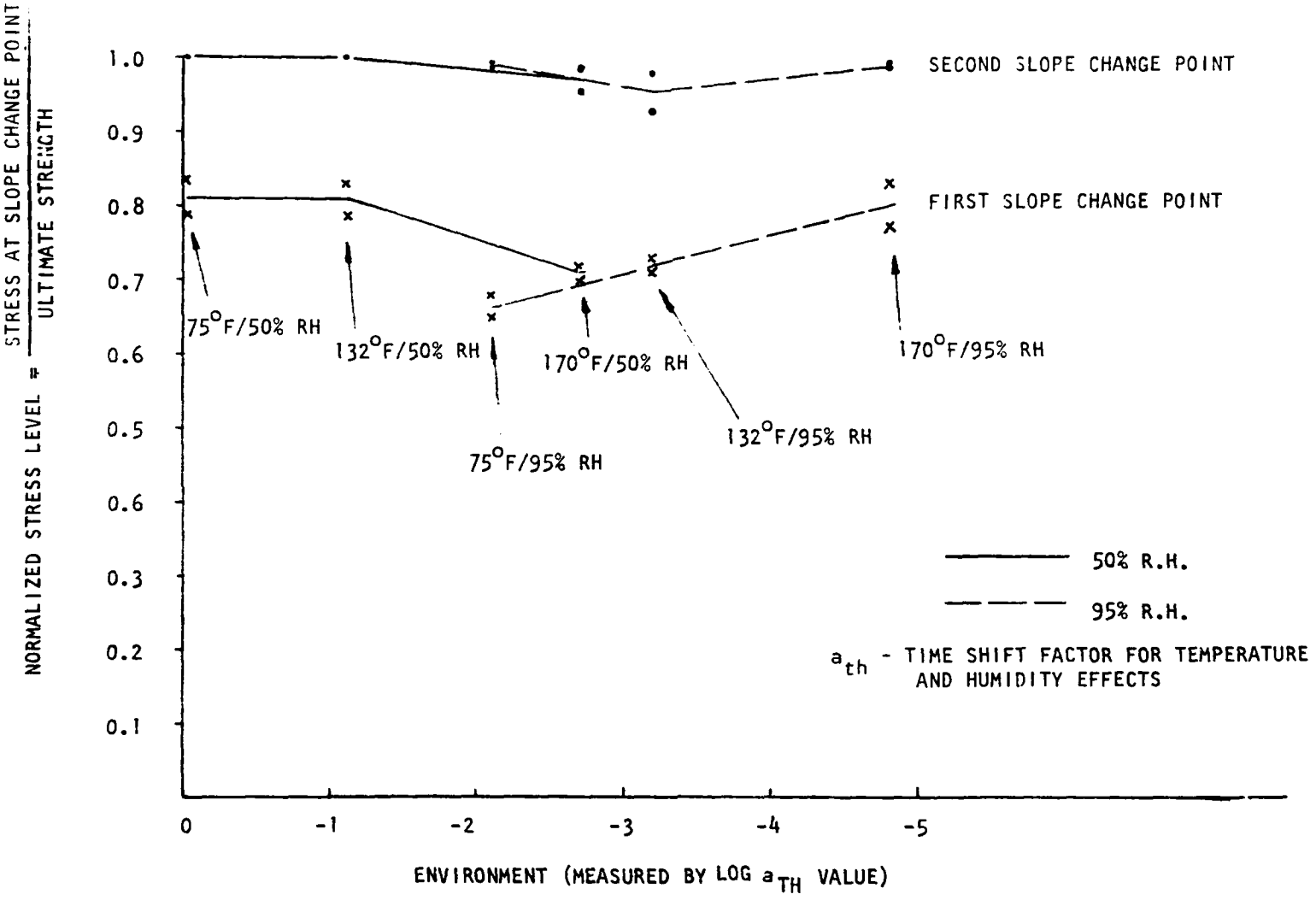

FIGURE 7. ENVIRONMENTAL EFFECTS ON STRESS AT SLOPE CHANGE POINTS FOR $(\pm 45/90_2)_s$ SPECIMENS

TABLE 8. DISTINCT SLOPE POINTS OF $(0/\pm45/90)_s$ STRESS-STRAIN CURVE

ENVIRONMENTS (°F/% RH)	SPECIMEN I.D.	DISTINCT SLOPE POINT		MODULI (MSI)	
		STRESS (psi)	STRAIN (μ IN/IN)	E_1	E_2
75/50	E1A7	40,909	5801	7.065	6.65
	E1A6	43,300	6060	7.198	6.49
132/50	E1B15	46,252	6577	7.038	6.36
	E1B14	43,977	6144	7.253	6.88
132/95	E1A10	56,282	7791	7.198	6.54
	E1A9	54,460	7531	7.213	6.73
170/50	E1B3	50,578	7185	7.087	6.51
	E1A8	47,612	6839	7.024	6.68

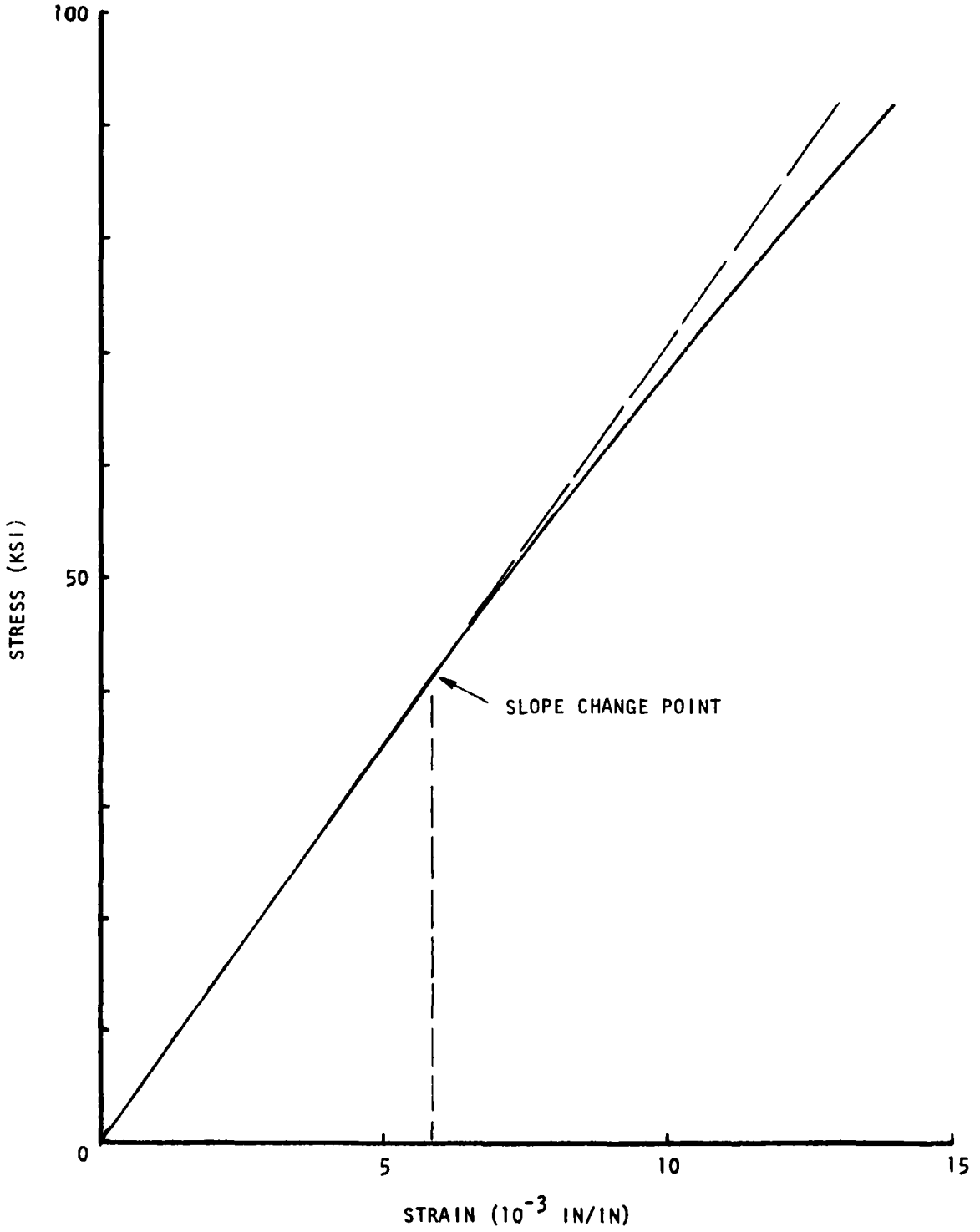

FIGURE 8. TYPICAL STRESS-STRAIN CURVE FOR $(0/\pm45/90)_s$ SPECIMEN AT 75°F/50%RH

In the laminate, the 0^{o}-ply (which is insensitive to environmental effects) is the primary load bearing ply and, thus, dominates the laminate properties. During initial loading in the Shore Western Machine, some 90^{o} plies started splitting (delamination) along the mid-plane (see Figures 9a and 9b) at around a 20,000 psi stress level (which is about 24% of the failure strength of the specimen). A retest of a dry specimen showed that the splitting of 90^{o} layers, Figure 9c, did not happen until the load was close to ultimate load. Thus, the failure mode of the $(0/\pm 45/90)_s$ specimen is influenced by the environment.

During Phase II and Phase III, four types of specimen layups were studies: $(90)_{20}$, $(\pm 45)_{2s}$, $(\pm 45/90_2)_s$ and $(0/\pm 45/90)_s$. For understanding in interpreting the specimen data, the edge effect in these specimens should be addressed. The edge effect which results from interlaminar shear or tension in a composite with a practical layup pattern has been identified as one of the primary failure mechanisms[4,5,6,7]. Wang and Crossman[4] examined a $(\pm 45)_s$ layup with the finite element technique to assess the high stress behavior of the edge area. The similarity of the deformation and boundary layer for $(\pm 45)_{2s}$ and $(\pm 45)_s$ have been compared by Pipes and Pagano[5]. In the linear range of the material and in a room temperature environment, the calculated maximum interlaminar tension is about 14% of the axial stress and the interlaminar shear stress is about 60% of the axial stress. Thus, interlaminar shear at the edge of the specimen may have a strong bearing on the crack initiation and failure of the $(\pm 45)_{2s}$ specimens.

To ascertain the impact on the edge effect in the failure of $(\pm 45/90_2)_s$ specimens, Pagano and Pipes[6] showed results for a $(\pm 40/90_2)_s$ specimen which is very similar to a $(\pm 45/90_2)_s$ specimen; their results indicated that the

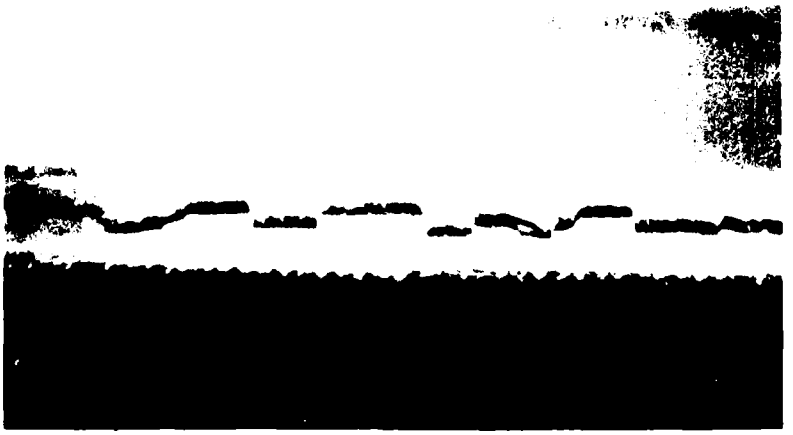

(a) 90^{o} Layers' Cracking in a 75°F/50% RH Environment

(b) Final Failure of $(0/\pm45/90)_s$ Due to 90^{o} Layers' Cracking

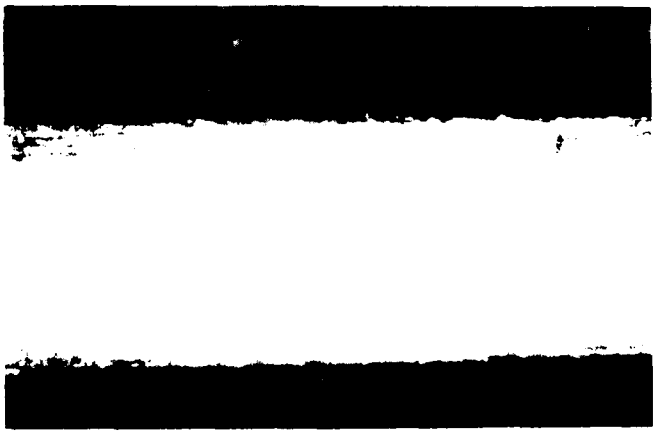

(c) On-Set of 90^{o} Layers' Cracking in Room Temperature Dry Environment

FIGURE 9. THE CRACKING OF 90^{o} LAYERS IN $(0/\pm45/90)_s$ SPECIMENS

delamination barely precedes ultimate failure. The interlaminar shear phenomenon for this type of specimen was not analyzed. The static failure behavior of the $(\pm 45/90_2)_s$ specimen indicates that the interlaminar shear effect between ± 45 plies is not as severe as that of the $(\pm 45)_2$ specimen at failure. The ultimate strain of the $(\pm 45)_s$ specimen is 90,000 μ in/in as compared with about 10,000 μ in/in for the $(\pm 45/90_2)_s$ specimen, where the 90^o lamina puts a lateral constraint on the $\pm 45^o$ laminae. The failed $(\pm 45/90_2)_s$ specimen does not show the necking down in the gage section, whereas the necking down is typical in the failure of $(\pm 45)_{2s}$ type specimens. Thus, 90^o laminae reduce the relative deformation between the +45 lamina and -45 lamina and reduce this particular interlaminar shear stress.

Statis tests indicated that the edge damage for the $(0/\pm 45/90)_s$ specimen is primarily from the interlaminar tension in the 90^o lamina (Figure 9). Edge delamination for the $(0/\pm 45/90)_s$ specimen at 60% of the average static strength has been observed by Ramani and Williams[7] and is considered by them to be the primary failure mechanism in their fatigue tests.

5.0 FATIGUE TESTS AND ANALYSIS

Experimental Observations

Fatigue tests were conducted for three types of specimens, $(90)_{20}$, $(\pm 45/90_2)_s$ and $(0/\pm 45/90)_s$. Pin type loading fixtures were used for the testing of $(90)_{20}$ and $(\pm 45/90_2)_s$ specimens. The $(0/\pm 45/90)_s$ specimens had additional clamp plates on the end tabs during testing which reinforced the bearing capability of the tab area. The $(\pm 45)_{2s}$ specimens (Table 1) were saved for later testing when a strain-controlled fatigue test capability becomes available; they will be tested during Phase IV. The temperature/humidity environments for the fatigue tests of various types of specimens are summarized in Table 9.

The fatigue test frequency was set at 3 Hertz with the load ratio being 0.1. Two specimens were tested at the same time. Specimens tested at one hydraulic station had a temperature sensor attached. The specimens tested at the other hydraulic station had both a temperature sensor and an extensometer. A diagram depicting the fatigue test set-up is shown in Figure 4. As discussed in Section 3.0, the displacement in each specimen is measured by an extensometer, and the LVDT signals in the extensometer are recorded on a strip chart recorder. The temperature in the specimen is monitored by the temperature sensor (ETG-50B from Micro-Measurements) and is recorded on the strip chart through the Vishay 2120 amplifier.

The fatigue test results at environments 75°F/50%RH, 132°F/50%RH, 132°F/95%RH, and 170°F/50%RH for $(\pm 45/90_2)_s$ are listed in Tables 10, 11, 12 and 13 respectively. Surface temperature data are included in these tables. Three peak fatigue stress levels, 50%, 55%, 60% of the ultimate static strength, were used.

TABLE 9. FATIGUE TEST ENVIRONMENTS

LAMINATE LAY-UP	ENVIRONMENTS (°F/% RH)							
	75/50	100/50	100/95	132/50	132/95	150/50	150/95	170/50
$(90)_{20}$		X	X			X	X	
$(\pm 45/90_2)_s$	X			X	X			X
$(0/\pm 45/90)_s$	X			X	X			X

TABLE 10. FATIGUE TEST RESULTS FOR $(\pm 45/90_2)_S$-SPECIMEN WITHIN A 75°F/50% R.H. ENVIRONMENT

SPECIMEN ID	FATIGUE STRESS		CYCLES	FAILURE MODE			RESIDUAL STRENGTH (PSI)	SURFACE TEMP. RISE (°F)	SPECIMEN QUALITY
	MAX. STRESS (PSI)	% OF F_{tU}		EDGE	GAGE	HOLE			
F2A2-5	10253	50	134668		X		-	9[b]	c
F2A2-6	10275	50	206442		X		-	10	c
F1B2-2	10273	50	23790		X		-	2[b]	c
F1B2-1	10273	50	32297		X		-	3[b]	c
F2B4-6	10278	50	62791		X		-	4	c
F2B3-3	10253	50	183751		X		-	3	c
F2A1-7	12330	60	2861		X		-	-	
F2A1-8	12480	60	6014	X			-	4	c
F2A2-1	12303	60	8952		X		-	4	c
F2A2-2	12306	60	27043		X		-	-	c
F2A2-3	12306	60	11076		X		-	-	c
F2A2-4	12306	60	32790		X		-	-	c
F2B4-7	11288	55	18308		X		-	3	c
F2B4-8	11288	55	9305		x		-	2	c

a. SPECIMEN DID NOT FAIL IN FATIGUE
b. TEMPERATURE SENSOR WAS ON THE FATIGUE FAILURE LOCATION
c. NO MACHINE DEFECTS
d. WITH MACHINE DEFECTS
e. WITH HIGH POROSITY
f. SPECIMEN THAT HAS BEEN CONDITIONED FOR (x) DAYS

TABLE 11. FATIGUE TEST RESULTS FOR $(\pm 45/90_2)_s$-SPECIMEN WITHIN A 132°F/50% R.H. ENVIRONMENT

SPECIMEN ID	FATIGUE STRESS		CYCLES	FAILURE MODE			RESIDUAL STRENGTH (PSI)	SURFACE TEMP. RISE (°F)	SPECIMEN QUALITY
	MAX. STRESS (PSI)	% OF F_{tU}		EDGE	GAGE	HOLE			
F3-8	10664	50	22773		X		-	5[b]	c
F3-7	10667	50	31130		X		-	5[b]	c
F2B2-2	10667	50	20440		X		-	7[b]	c
F2B3-1	10652	50	38780		X		-	6[b]	c
F2B3-5	10632	50	24347		X		-	6[b]	c
F2B3-4	10651	50	21166		X		-	5	c
F2A2-7	12872	60	4106		X		-	3	c
F2A2-8	12796	60	593		X		-	4[b]	c
F1B2-3	12792	60	2390		X		-	5[b]	c
F2B1-4	12788	60	1361		X		-	2	c
F1B2-5	12804	60	1736		X		-	4	c
F1B2-6	12788	60	1710		X		-	-	c
F3-16	11744	55	7566		x		-	4	c
F3-15	11744	55	7942		x		-	4	c
F3-14	11696	55	6188	x			-	4	c
F3-13	11727	55	6890		x		-	9[b]	c

a. SPECIMEN DID NOT FAIL IN FATIGUE
b. TEMPERATURE SENSOR WAS ON THE FATIGUE FAILURE LOCATION
c. NO MACHINE DEFECTS
d. WITH MACHINE DEFECTS
e. WITH HIGH POROSITY
f. SPECIMEN THAT HAS BEEN CONDITIONED FOR (x) DAYS

TABLE 12. FATIGUE TEST RESULTS FOR $(\pm 45/90_2)_s$-SPECIMEN WITHIN A 132°F/95% R.H. ENVIRONMENT

SPECIMEN ID	FATIGUE STRESS		CYCLES	FAILURE MODE			RESIDUAL STRENGTH (PSI)	SURFACE TEMP. RISE (°F)	SPECIMEN QUALITY
	MAX. STRESS (PSI)	% OF F_{tU}		EDGE	GAGE	HOLE			
F2A1-1	8485	50	129692		X		-	4	c
F2A1-2	8460	50	114765		X		-	3	c
F2A1-3	8469	50	132538		X		-	5	c
F2A1-4	8469	50	62482		X		-	3[b]	c
F1B1-1	8455	50	52874		X		-	2	c
F1B1-2	8455	50	38515		X		-	3	c
F1A2-3	10144	60	7578		X		-	5	c
F1A2-4	10158	60	6665		X		-	4	c
F1A2-5	10158	60	7818		X		-	2	c
F1A2-6	10163	60	5170		X		-	3	c
F1A2-7	10140	60	8304		X		-	2	c
F1A2-8	10160	60	6060		X		-	3	c
F1B1-7	9312	55	15300		x		-	3[b]	c
F1B1-8	9278	55	10089		x		-	4	c
F1B1-5	9303	55	14163	x			-	2	c
F1B1-6	9278	55	8124		x		-	2	c
F1B104	9303	55	9411	x			-	2	c
F1B1-3	9303	55	11505		x		-	1	c

a. SPECIMEN DID NOT FAIL IN FATIGUE
b. TEMPERATURE SENSOR WAS ON THE FATIGUE FAILURE LOCATION
c. NO MACHINE DEFECTS
d. WITH MACHINE DEFECTS
e. WITH HIGH POROSITY
f. SPECIMEN THAT HAS BEEN CONDITIONED FOR (x) DAYS

TABLE 13. FATIGUE TEST RESULTS FOR $(\pm 45/90_2)_s$-SPECIMEN WITHIN A 170°F/50% R.H. ENVIRONMENT

SPECIMEN ID	FATIGUE STRESS		CYCLES	FAILURE MODE			RESIDUAL STRENGTH (PSI)	SURFACE TEMP. RISE (°F)	SPECIMEN QUALITY
	MAX. STRESS (PSI)	% OF F_{tU}		EDGE *	GAGE +	HOLE			
F3-1	9282	50	115856		X		-	6[b]	c
F3-2	9282	50	73106	X			-	5[b]	c
F3-3	9282	50	58574		X		-	3	c
F3-4	9282	50	50249		X		-	1	c
F3-6	9282	50	103807	X			-	2	c
F3-5	9292	50	134795		X		-	-	c
F1B2-7	11138	60	4085		X		-	5	c
F1B2-8	11121	60	3365		X		-	-	c
F2B4-1	11148	60	9539		X		-	11[b]	c
F2B4-2	11121	60	5896		X		-	-	c
F2B4-3	11121	60	7213		X		-	10	c
F2B4-4	11121	60	5986		X		-	-	c
F2B3-7	10215	55	14753		x		-	-	c
F2B3-8	10242	55	11375	x			-	-	c
F2B4-5	10212	55	10797		x		-	-	c
F2B4-6	10220	55	14755	x			-	-	c

a. SPECIMEN DID NOT FAIL IN FATIGUE
b. TEMPERATURE SENSOR WAS ON THE FATIGUE FAILURE LOCATION
c. NO MACHINE DEFECTS
d. WITH MACHINE DEFECTS
e. WITH HIGH POROSITY
f. SPECIMEN THAT HAS BEEN CONDITIONED FOR (x) DAYS

+ * See Table 5 for Definition

Most of the fatigue failures of the $(\pm 45/90_2)_s$ specimens occurred within the specimen gage area (Table 13). The temperature increase on the specimen surfaces was measured using temperature gages and was found to be within the 2^o - 5^oF range. The maximum temperature increase observed was 11^oF. The fatigue strain history for the $(\pm 45/90_2)_s$ specimens was monitored by the extensometer. The mean fatigue strains at various environments are shown in Figures 10 to 13 and the strain amplitudes ($\frac{1}{2}$ peak-to-peak) are shown in Figures 14 to 17, where different symbols indicate a different specimen at each loading environment. By using these fatigue strain data and comparing them with the static stress-strain curve from Figure 6, the fatigue failure process can be interpreted. Since the maximum fatigue stress level was 60% of the ultimate strength, which is under the minimum 65% level that is required for the 90^o ply to start cracking (according to the static results in Figures 6 and 7), the $(\pm 45/90_2)_s$ specimens were considered structurally sound at the beginning of the fatigue test. Edge effect as discussed in Section 4.0 does not cause edge cracks at 60% ultimate stress level. As the fatigue cycling continues, the strain level gradually increases due to the effect of the mean fatigue load. The S/N curves are shown in Figure 18, excluding data from specimens which failed at holes.

Test environments for $(0/\pm 45/90)_s$ specimens are shown in Table 9. The mechanical properties of the $(0/\pm 45/90)_s$ layup are considerably stronger than those of the $(\pm 45/90_2)_s$ layup, as shown in Table 6. The tabs with pins and adhesive can take static loads up to 2700 lbs. During fatigue loading, the adhesive could not always take the oscillatory load. Shear-out failure of the laminate from the tab area around the pin hole is common in the $(0/\pm 45/90)_s$ specimens, especially in the high humidity environment. Moisture-induced degradation of the adhesive in the tab areas was suspected for this type of hole failure mode.

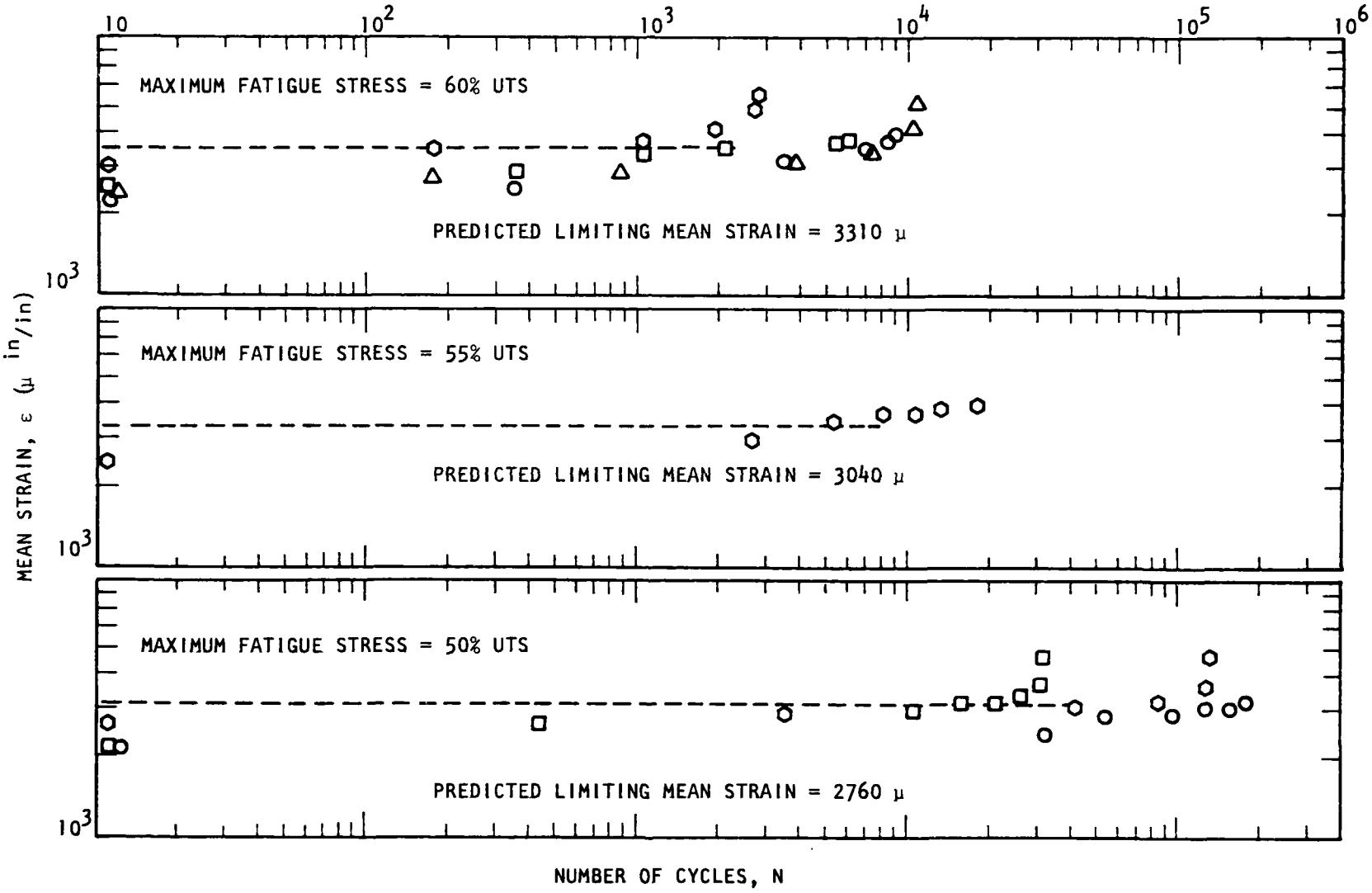

FIGURE 10. MEAN FATIGUE STRAIN CURVE OF $(\pm 45/90_2)_s$ SPECIMEN AT 75°F/50% RH ENVIRONMENT

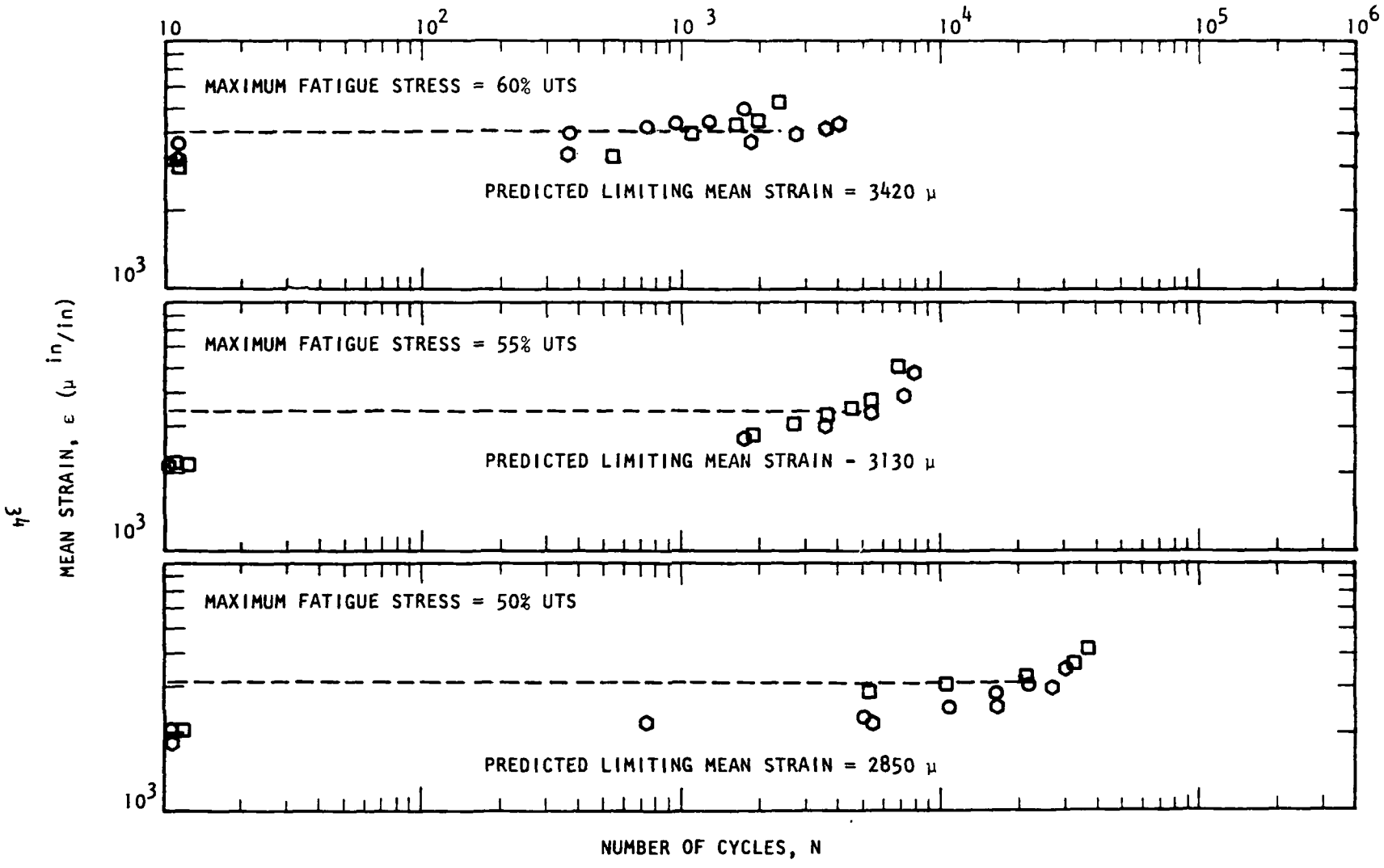

FIGURE 11. MEAN FATIGUE STRAIN CURVE OF $(\pm 45/90_2)_s$ SPECIMEN AT 132°F/50% RH ENVIRONMENT

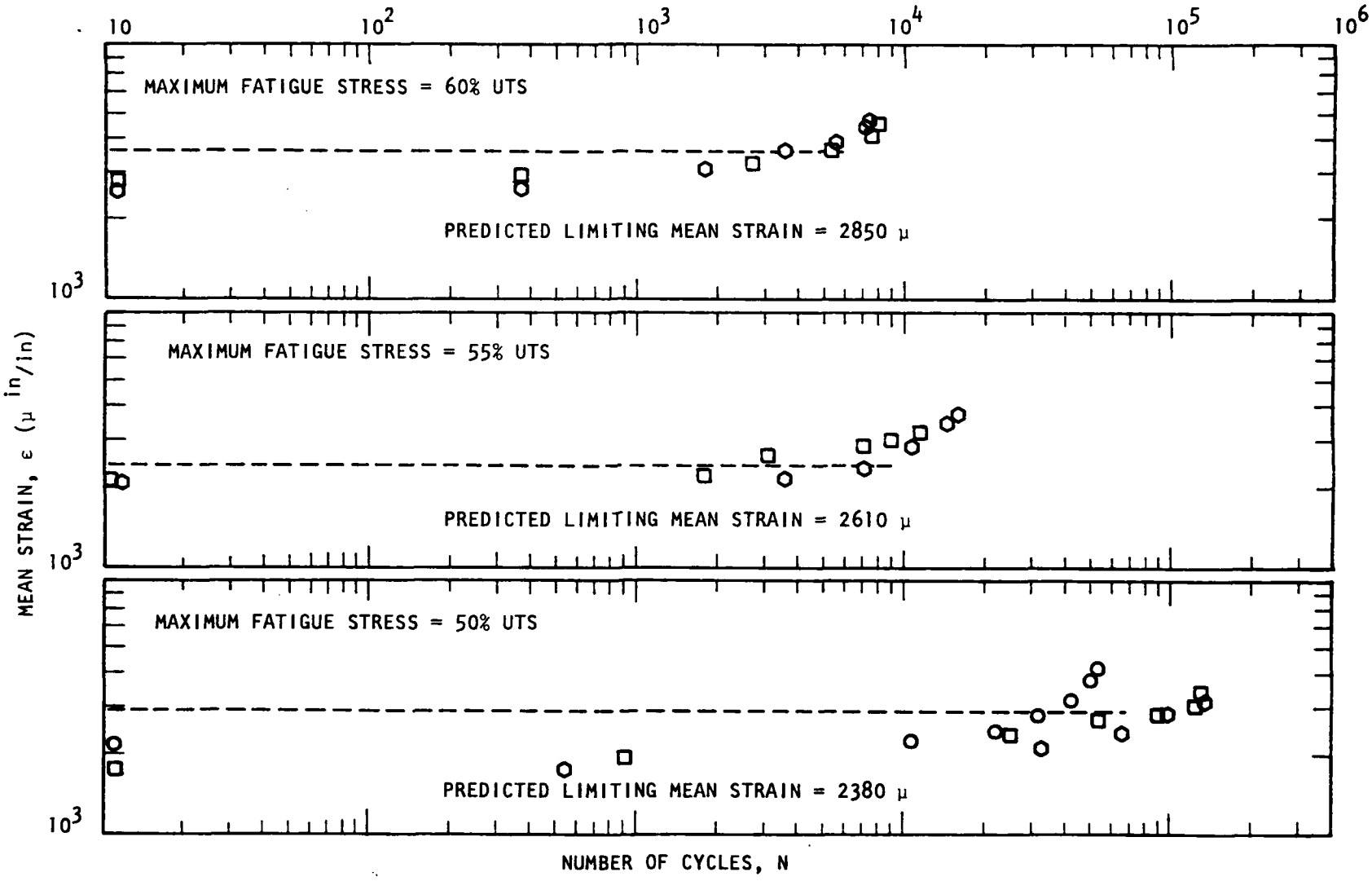

FIGURE 12. MEAN FATIGUE STRAIN CURVE OF $(\pm 45/90_2)_s$ SPECIMEN AT 132°F/95% RH ENVIRONMENT

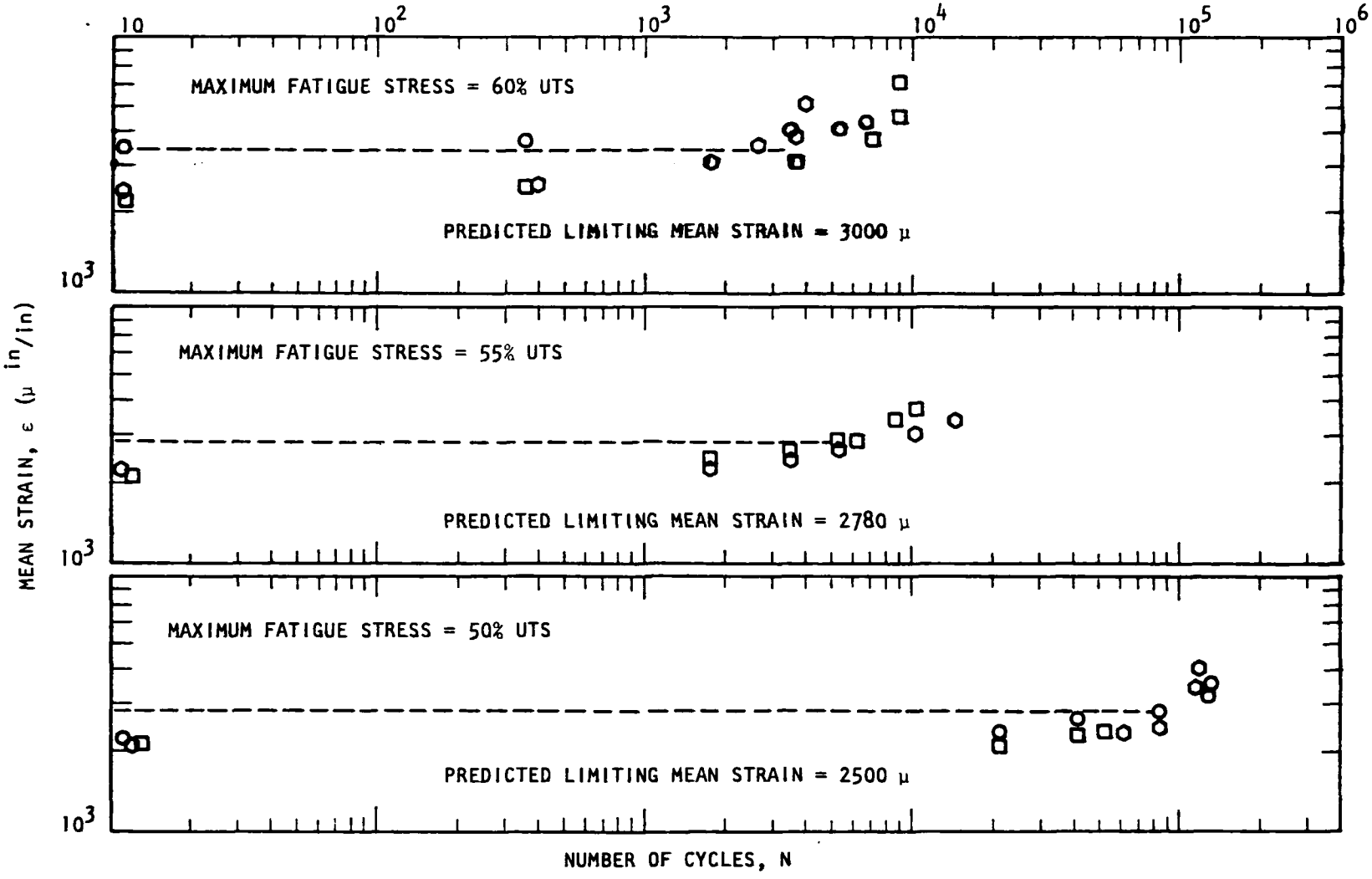

FIGURE 13. MEAN FATIGUE STRAIN CURVE OF $(\pm 45/90_2)_s$ SPECIMEN AT 170°F/50% RH ENVIRONMENT

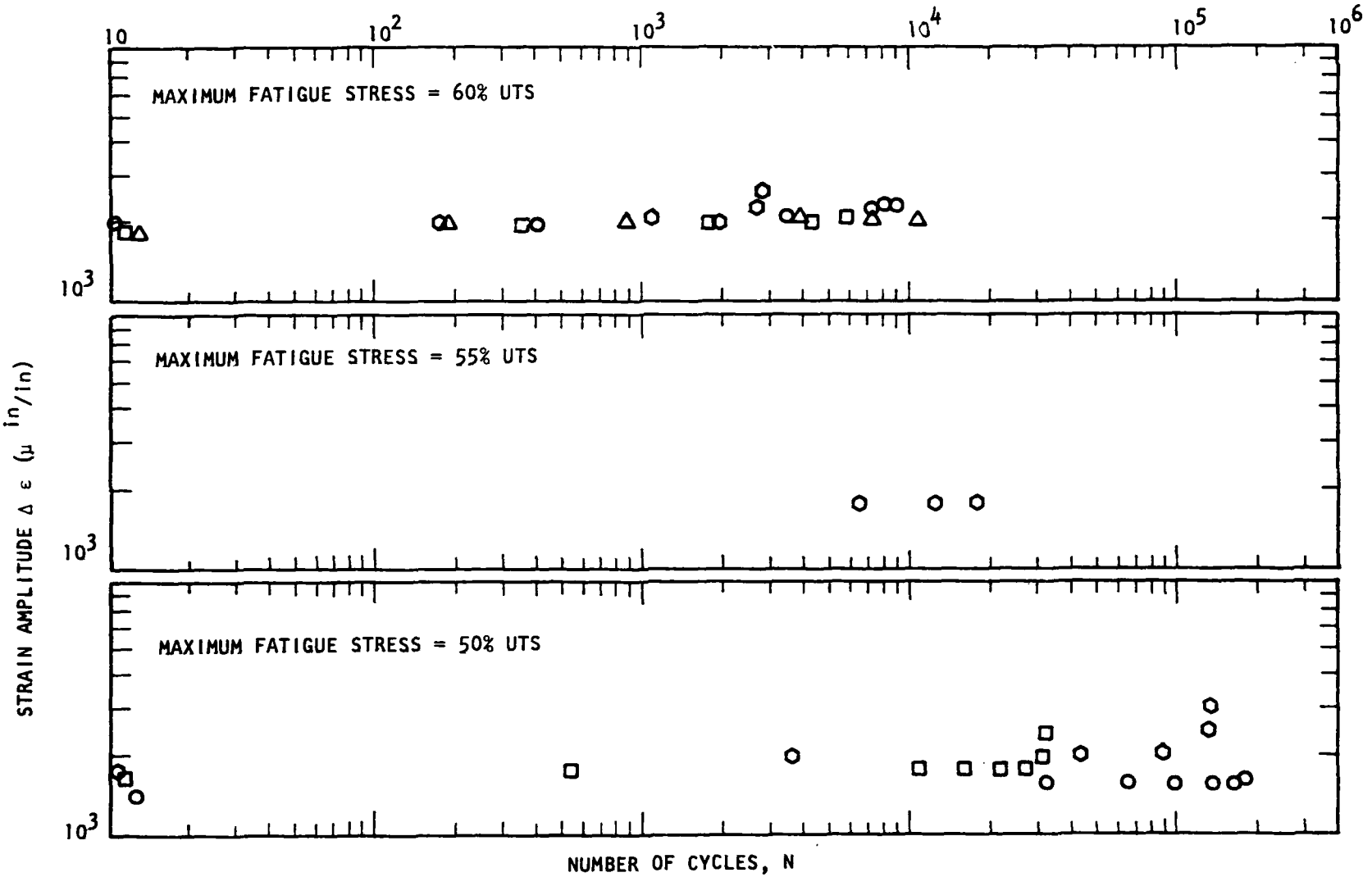

FIGURE 14. STRAIN AMPLITUDE OF $(\pm 45/90_2)_s$ SPECIMEN AT 75°F/50% RH ENVIRONMENT

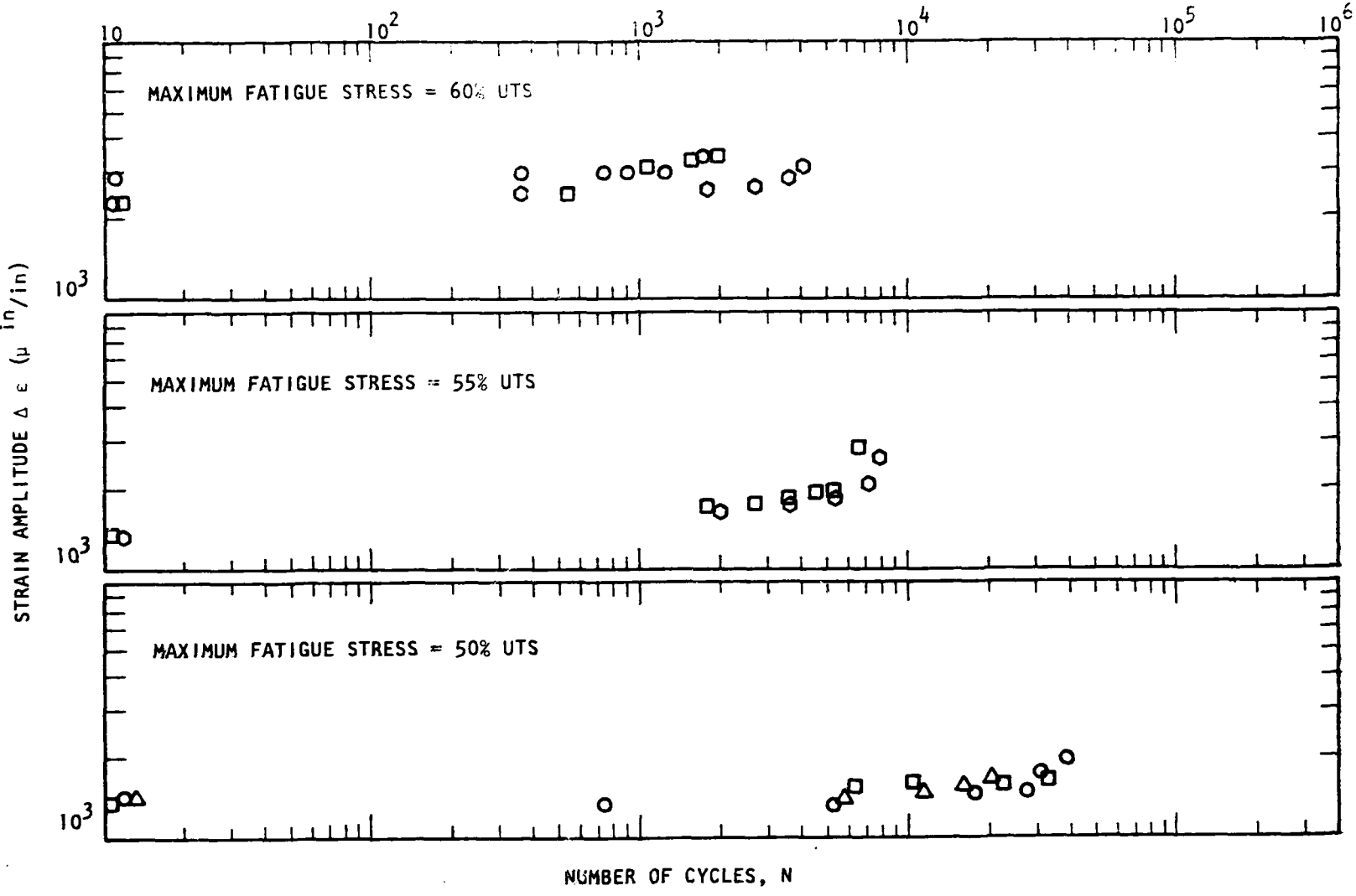

FIGURE 15. STRAIN AMPLITUDE OF $(\pm 45/90_2)_s$ SPECIMEN AT 132°F/50% RH ENVIRONMENT

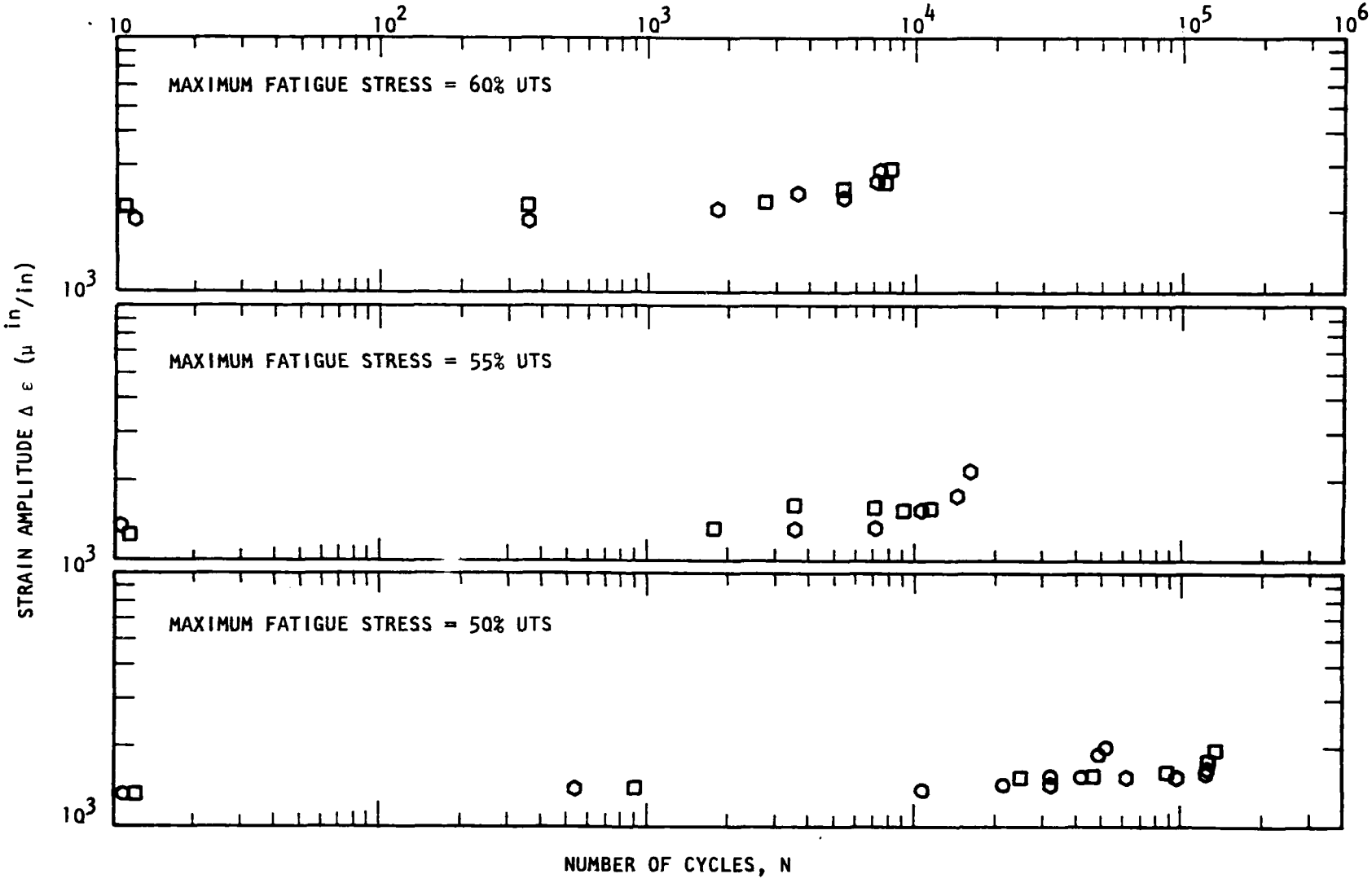

FIGURE 16. STRAIN AMPLITUDE OF $(\pm 45/90_2)_s$ SPECIMEN AT 132°F/95% RH ENVIRONMENT

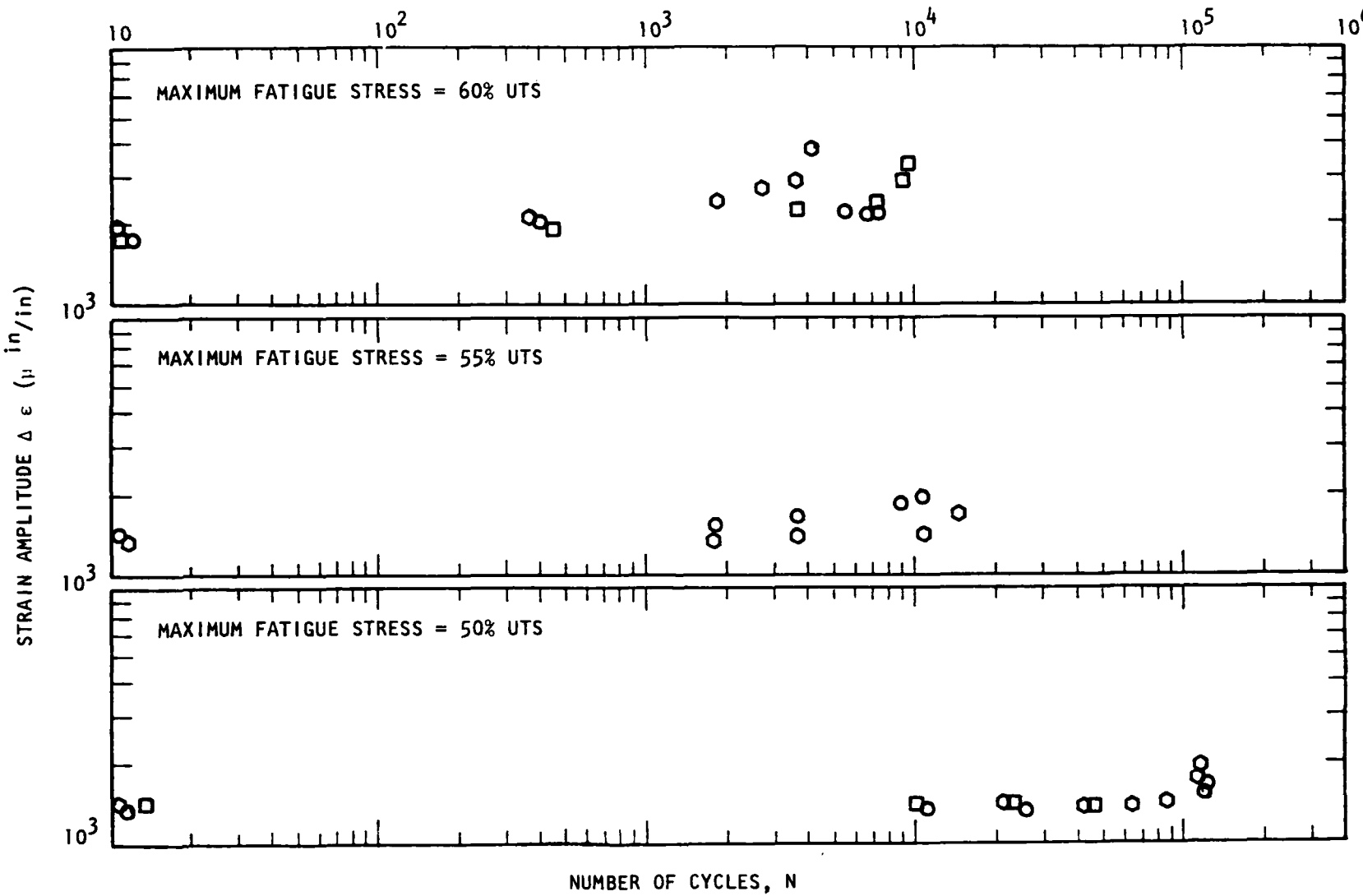

FIGURE 17. STRAIN AMPLITUDE OF $(\pm 45/90_2)_s$ SPECIMEN AT 170°F/50% RH ENVIRONMENT

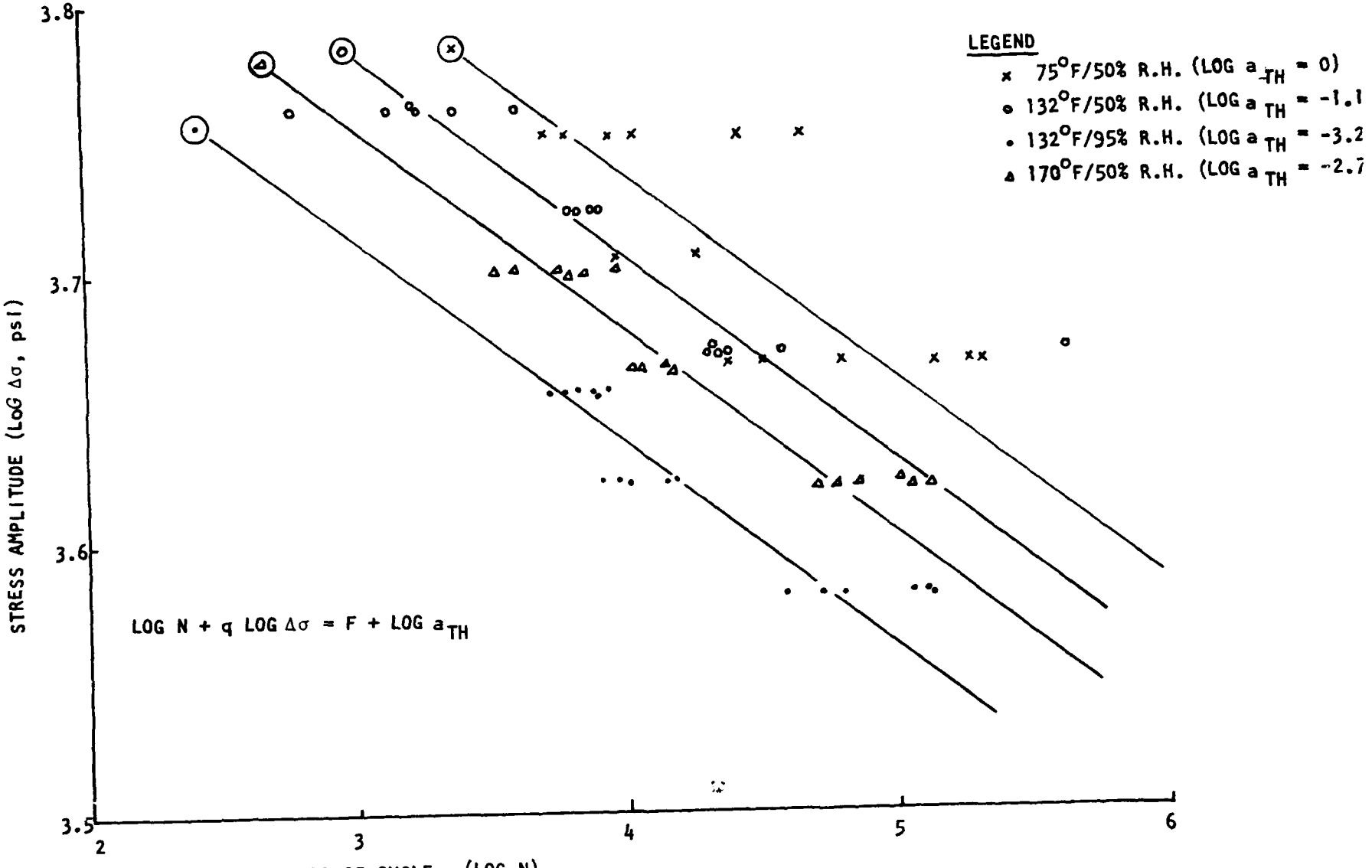

FIGURE 18. THE S-N CURVE OF $(\pm 45/90_2)_s$ SPECIMENS WITHIN FOUR ENVIRONMENTS

To verify this and to generate fatigue data, thirty-six more specimens of $(0/\pm45/90)_s$ layup were fabricated (from Panel E_3 in the Table 1) for environmental conditioning and testing. The end tab area on these new specimens was protected by wrapping it with aluminum backing tape, which provides better protection against moisture than the Mylar scotch tape. Test results on these thirty-six specimens showed only minor improvement in reducing fatigue failure in the hole area. The 95% R.H. conditioned specimens could not take the fatigue loading. Without these hole failure data, the fatigue results for the $(0/\pm45/90)_s$ specimens are shown in Tables 14-16 with surface temperature data included. Environments 75°F/50%RH and 130°F/50%RH provided more fatigue data points because hole failure was less common in these two environments. Figures 19-22 show the mean strain and strain amplitude histories in fatigue cycling. It is noted that the middle 90° layers split in most of the $(0/\pm45/90)_s$ specimens in their first hundred cycles. Figures 19 and 20 indicate that creep strain exists even in the fiber-dominated laminate construction. The S-N curve is shown in Figure 23.

Some 90° specimen fatigue tests were conducted at 100°F/50%RH, 100°F/95%RH and 150°F/50%RH environments. As seen in the static test results from Table 5, the strengths of 90° specimens are about 15% higher than those in the Phase II program. Fatigue data of the 90° specimens conducted during Phase II and Phase III are not directly comparable without further study. Hence, current fatigue data for the 90° specimens and their analysis will not be reported. For reference purposes in the following discussion, the S-N curves for $(90^\circ)_{20}$ and $(\pm45)_{2s}$ specimens from Phase II are reproduced in Figure 24 and Figure 25.

Experimental-Theoretical Correlations

In Phase I, the creep behavior of different laminates at low stresses was related to the in situ creep compliance of the matrix[1] using standard equations

TABLE 14. FATIGUE TEST RESULTS FOR $(0/\pm45/90)_s$ SPECIMENS

ENVIRONMENT (°F/% RH)	SPECIMEN ID	FATIGUE STRESS		CYCLES	FAILURE MODE		SURFACE TEMPERATURE RISE (°F)
		MAX. STRESS (PSI)	% of F_{tu}		EDGE	GAGE	
75/50	E2B-12	72455	80	172		X	-
	E2B-13	72443	80	1126		X	-
	E2A-13	72430	80	1256		X	4
	E2A-14	72453	80	548		X	5
	E2A-15	72533	80	49		X	-
	E2A-16	72344	80	306		X	4
	E1B-20	70648	78	147		X	-
	E2B-2	67988	75	293		X	5
	E2B-3	67847	75	740		X	4
	E2B-4	67988	75	224		X	4
	E2B-5	67847	75	167		X	1
	E1B-21	65213	72	5163		X	8
	E2A-21	64172	71	9494		X	8
	E2A-19	63375	70	17793		X	6
	E2A-20	63392	70	15117	X		7
	E2A-3	58841	65	9296		X	4
	E2A-4	58841	65	6230		X	9
	E2B-14	58854	65	36315		X	4
	E2B-15	58854	65	10680		X	7
	E2A-5	58854	65	7270		X	6
	E2A-6	58854	65	7753	X		7
	E3-20	58844	65	43774	X		-
	E2A-11	50943	56	321500		X	-
	E2A-12	50947	56	196700		X	-

TABLE . FATIGUE TEST RESULTS FOR [illegible] SPECIMENS

ENVIRONMENT (°F/% RH)	SPECIMEN ID	FATIGUE STRESS		CYCLES	FAILURE MODE		SURFACE TEMPERATURE RISE (°F)
		MAX. STRESS (PSI)	T of F_{tu}		EDGE	GAGE	
	E1B-16	64356	80	534		X	4
	E1B-17	64373	80	1821		X	5
	E1B-19	64356	80	177		X	-
	E3-5	56312	70	17642	X		6
	E3-6	56312	70	810	X		-
	E3-[illegible]	56332	70	23064		X	-
	E3-[illegible]	56299	70	24242		X	2
	E3-9	56197	70	2018		X	-
	E3-10	52298	65	161862		X	10
	E3-11	52380	65	95850		X	-
	E3-12	52380	65	49144	X		2
	E3-15	52285	65	140136		X	-
	E3-17	48257	60	608258	X		-
	E3-22	48257	60	83709	X		-
	E3-24	48262	60	24236		X	-
	E3-25	48260	60	920469		X	2
	E3-26	48260	60	451757		X	-
	E3-27	48286	60	52743	X		2
	E3-28	48262	60	418191	X		-
	E3-29	48257	60	178984		X	-

TABLE 16. FATIGUE TEST RESULTS FOR $(0/\pm45/90)_S$ SPECIMENS

ENVIRONMENT (°F/%RH)	SPECIMEN ID	FATIGUE STRESS		CYCLES	FAILURE MODE		SURFACE TEMPERATURE RISE (°F)
		MAX STRESS (PSI)	% OF F_{tu}		EDGE	GAGE	
	E2B-18	50957	65	260206		X	3
	E2B-19	51129	65	272906		X	5
75/95	E2B-17	50314	64	129600		X	8
	E3-32	50938	65	11465		X	-
132/95	E3-33	50938	65	129117		X	2

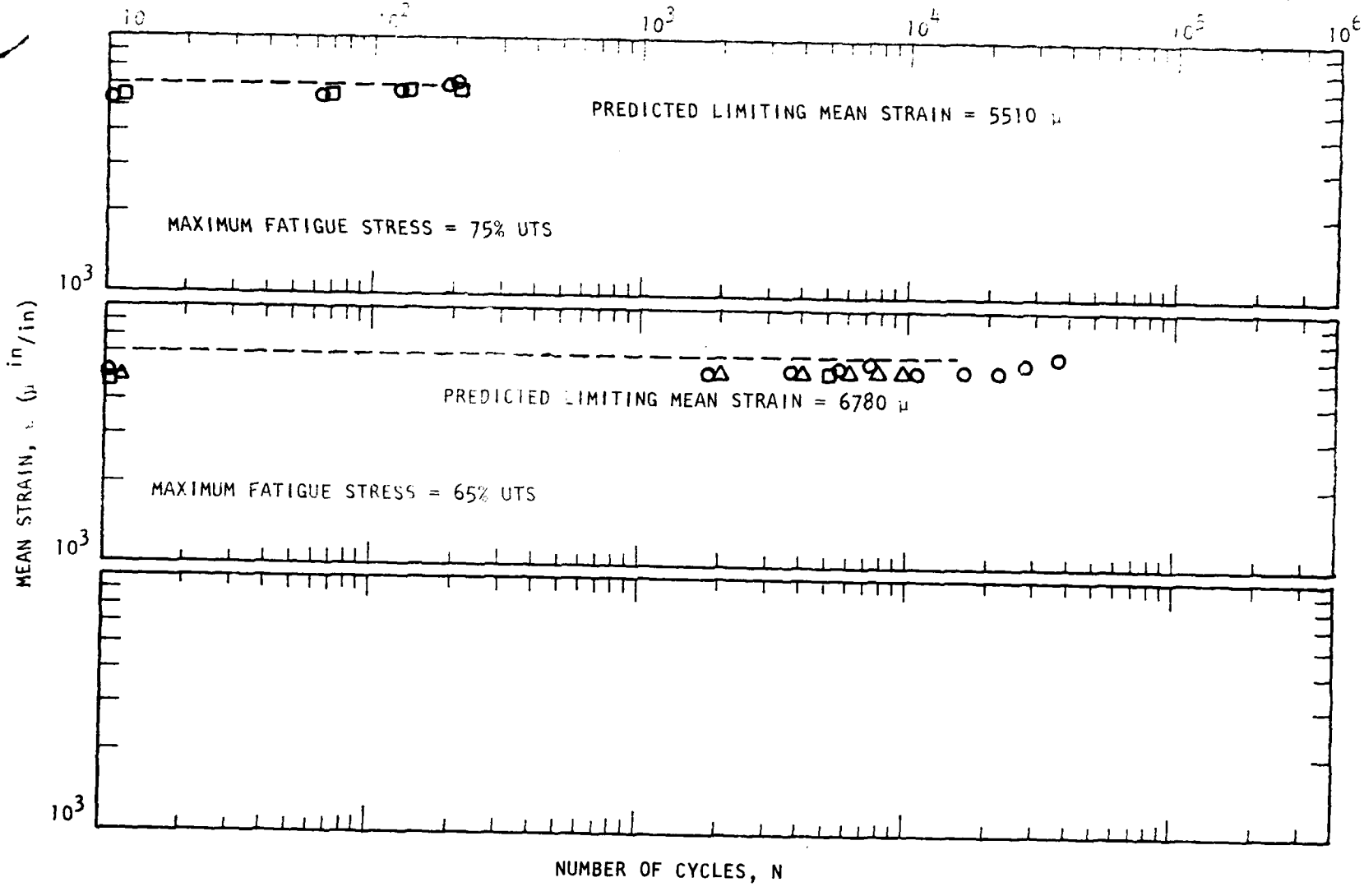

FIGURE 19. MEAN FATIGUE STRAIN CURVE OF $(0/\pm45/90)_s$ SPECIMEN AT 75°F/50% RH ENVIRONMENT

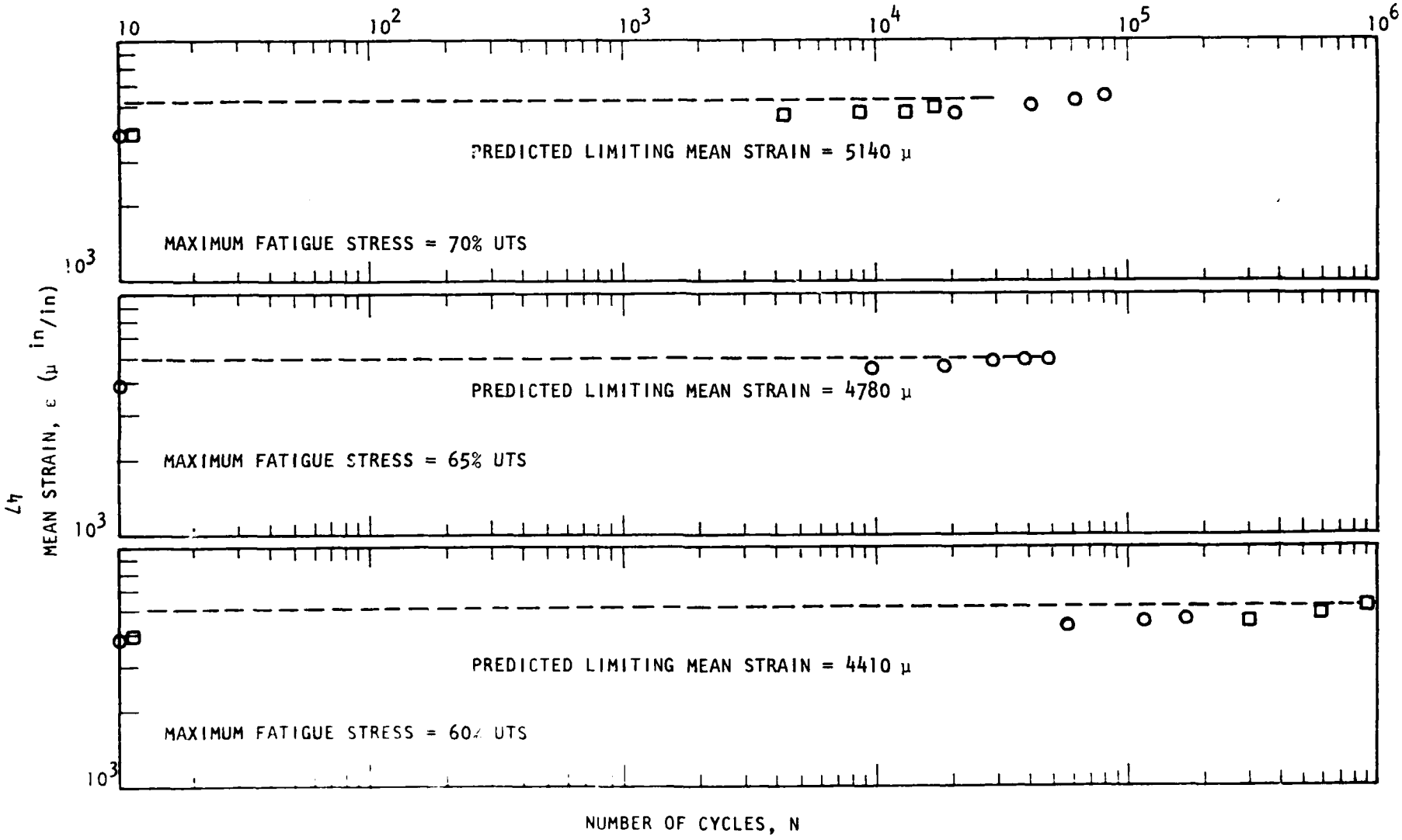

FIGURE 20. MEAN FATIGUE STRAIN CURVE OF $(0/\pm45/90)_s$ SPECIMEN AT 132°F/50% RH ENVIRONMENT

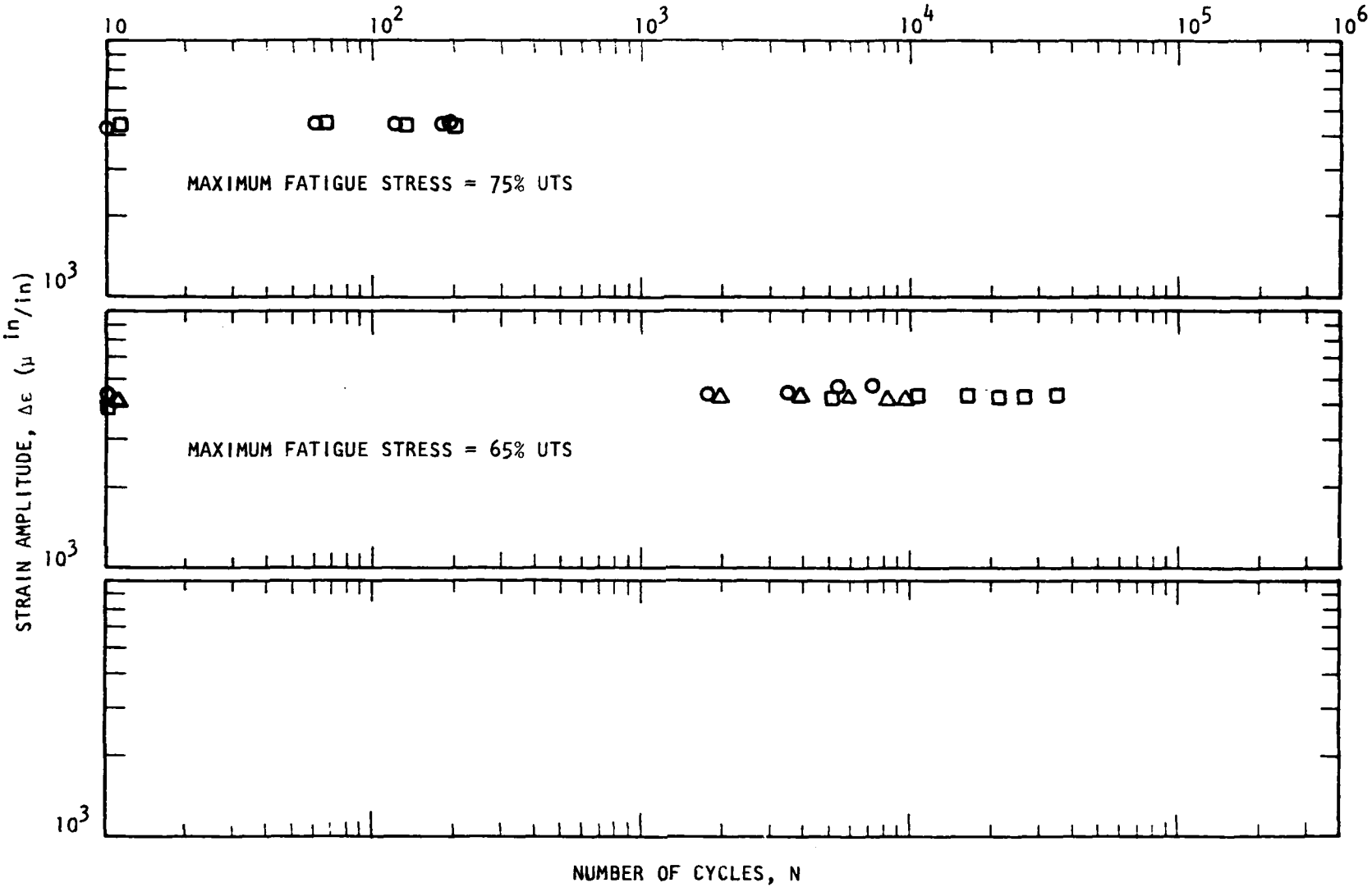

FIGURE 21. STRAIN AMPLITUDE OF $(0/\pm45/90)_s$ SPECIMEN AT 75°F/50% RH ENVIRONMENT

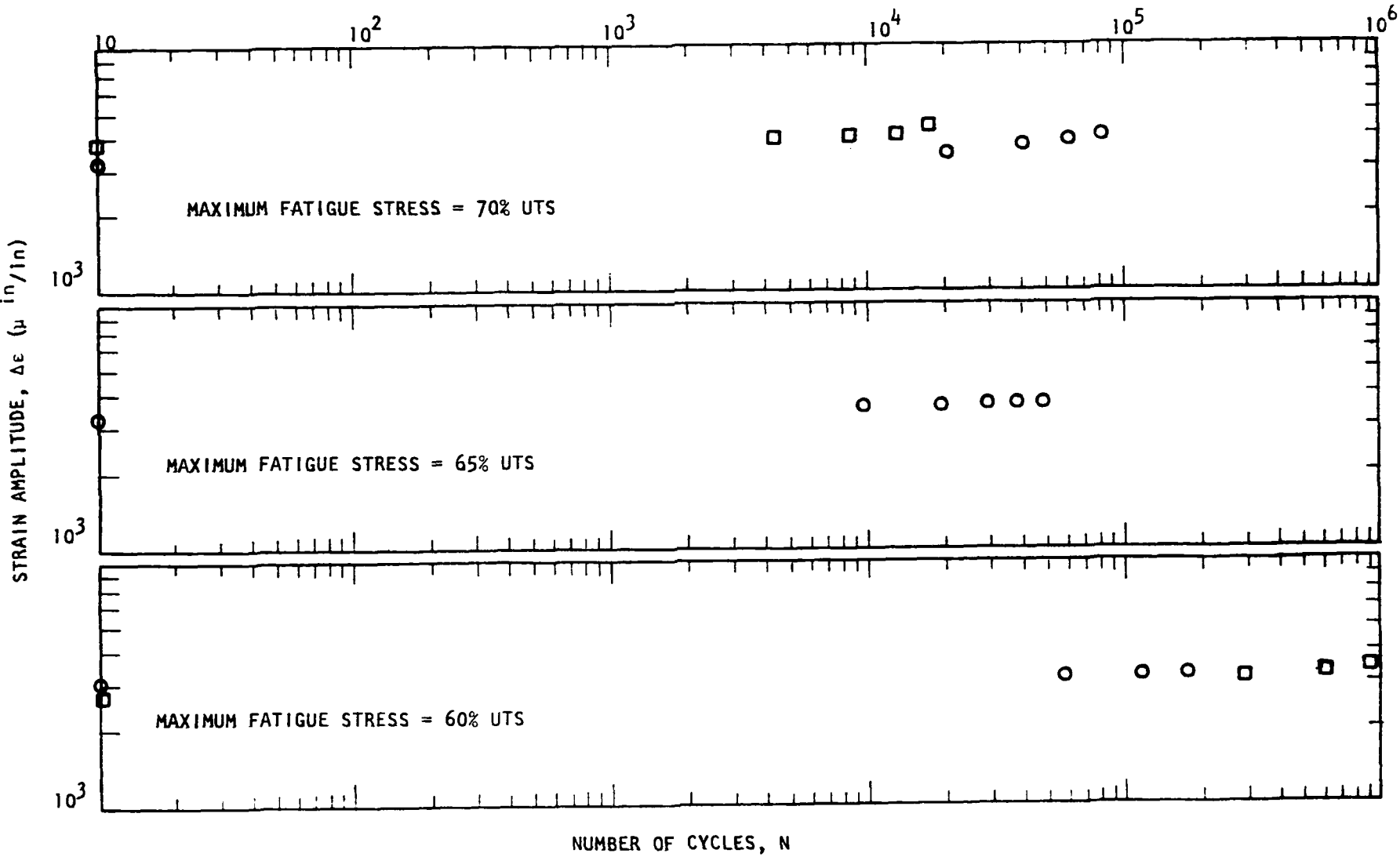

FIGURE 22. STRAIN AMPLITUDE OF $(0/\pm45/90)_x$ SPECIMEN AT 132°F/50% RH ENVIRONMENT

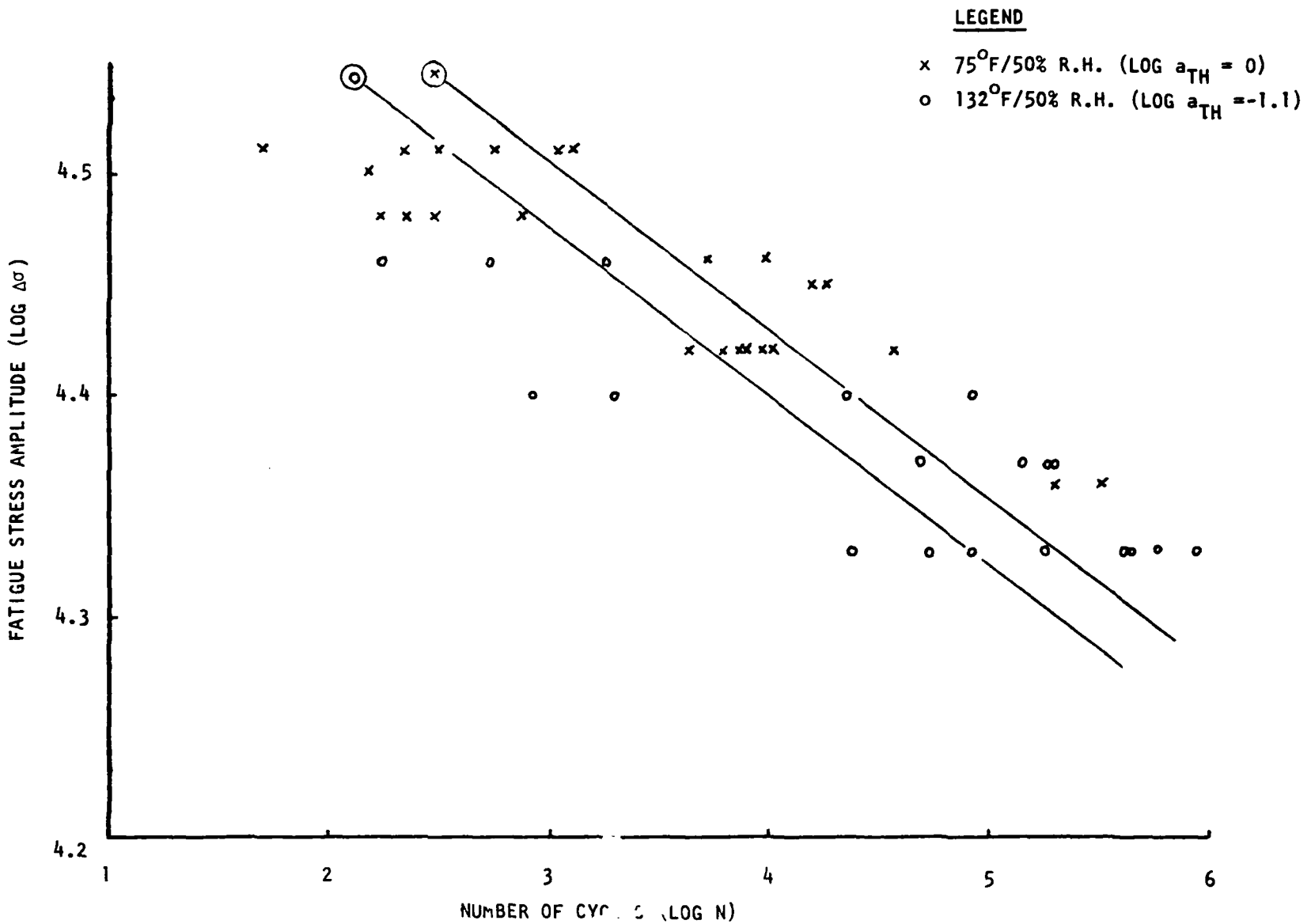

FIGURE 23. THE S-N CURVE OF $(0/\pm45/90)_S$ SPECIMEN AT TWO ENVIRONMENTS

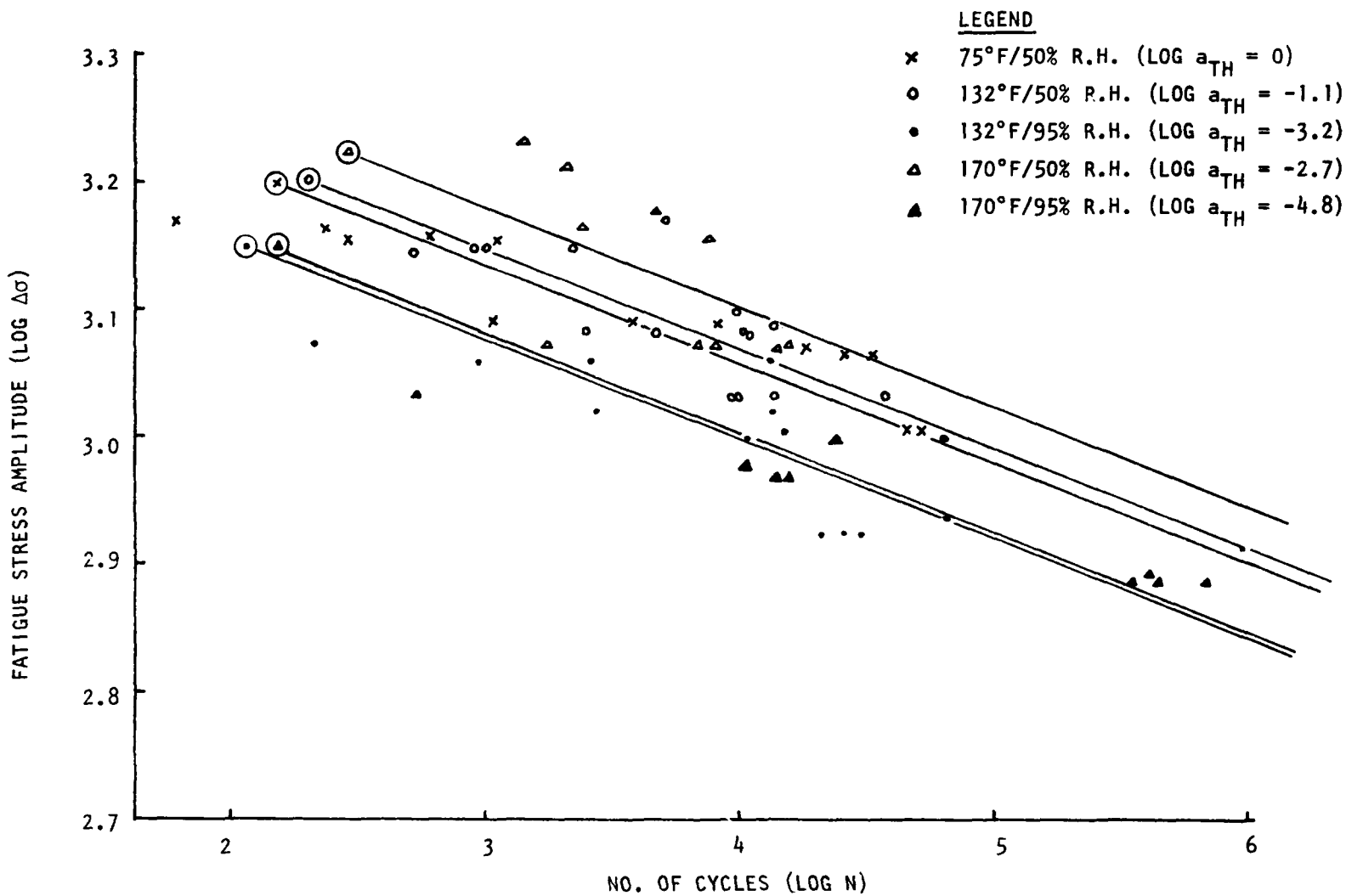

FIGURE 24. THE S-N CURVE OF 90°-SPECIMEN AT VARIOUS ENVIRONMENTS

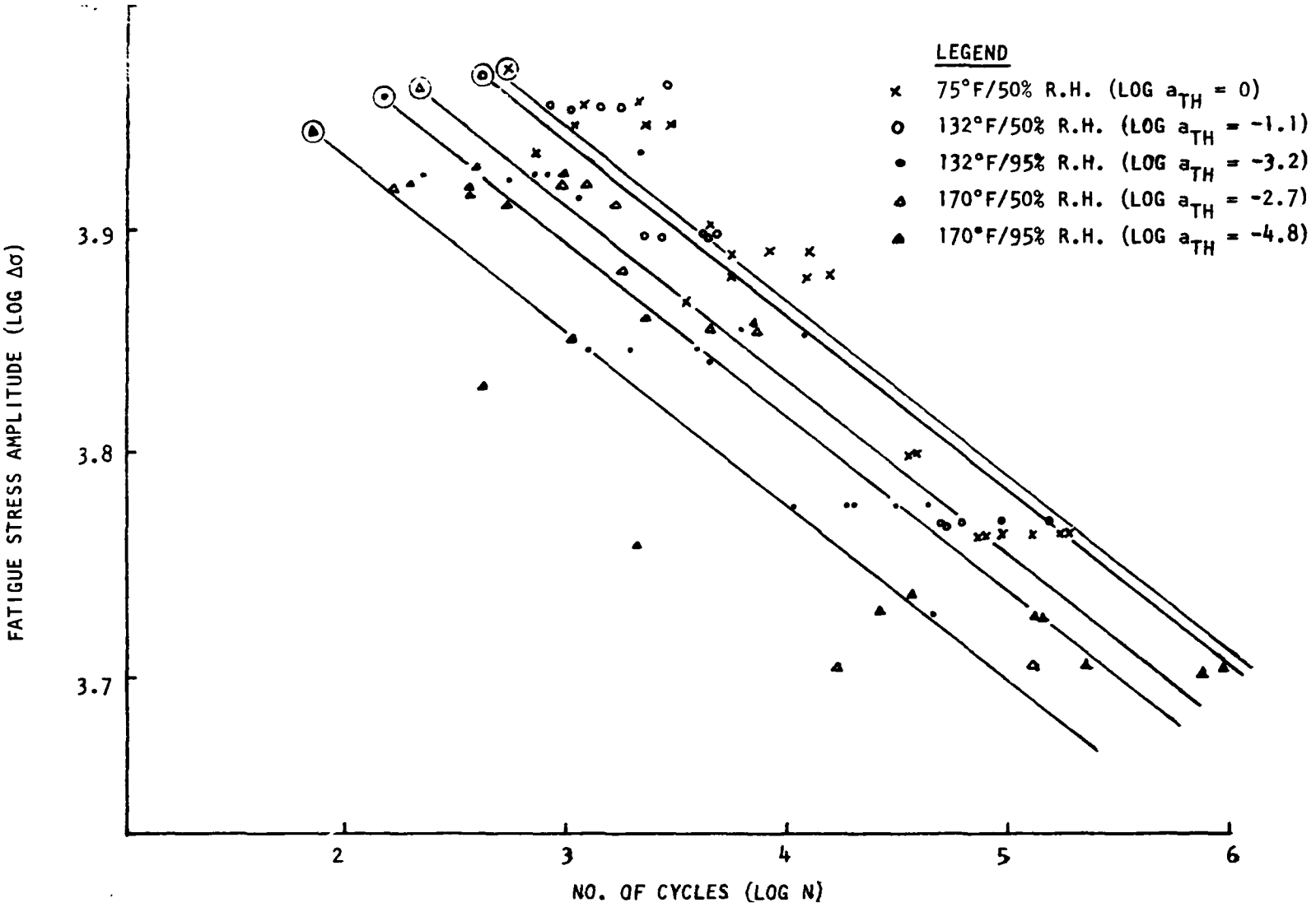

FIGURE 25. THE S-N CURVE OF ±45°-SPECIMEN AT VARIOUS ENVIRONMENTS

based on micromechanics and laminate theory for elastic media. By this procedure, it was possible to correlate laminate creep behavior for various environments in terms of a single master matrix creep curve and temperature and moisture-dependent shift factors for the matrix. For structural design purposes, one would reverse the process and use the constituent fiber and matrix properties to predict creep response of an arbitrary laminate by means of micromechanics and lamination theory.

A fatigue and fracture theory for viscoelastic composites should be capable of providing similar correlations and predictions. In this section, we shall demonstrate that some aspects of the fatigue and static fracture data given in the report can be correlated using the same equations as employed in the creep theory. This study will add in understanding the observed laminate behavior and in providing a basis for the development of a physically-based fatigue theory.

Compliance predictions have been made in which constituent properties for the $(\pm 45)_{2s}$ and $(90)_{20}$ laminates found from Phase I were used. The results are given in Figures 26 and 27 for the compliance in the direction of loading. Figure 26 shows the laminate compliance as a function of matrix compliance, for the four laminates employed in the fatigue tests. For ease of later comparison with data, compliance curves for the $(\pm 45/90_2)_s$ and $(0/\pm 45/90)_s$ laminates are converted to modulus curves in Figure 27. A limiting modulus exists for both the $(\pm 45/90_2)_s$ and $(0/\pm 45/90)_s$ laminates when $E_M = 0$; these limiting moduli are actually those for a fiber network in which the matrix does not support any in-plane load. The matrix serves only to maintain a condition of uniform

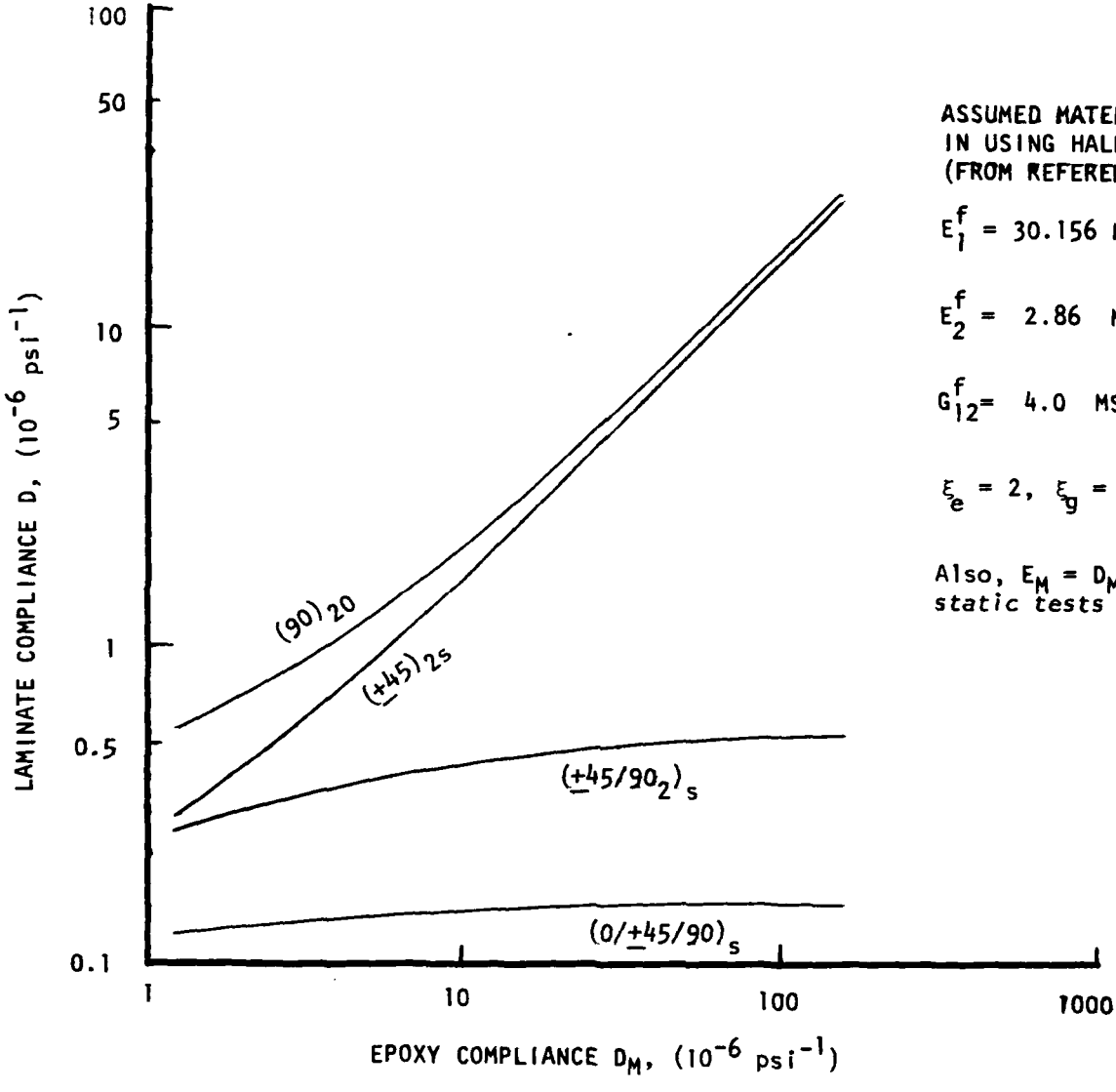

ASSUMED MATERIAL CONSTANTS IN USING HALPIN-TSAI EQUATIONS (FROM REFERENCE 1):

E_1^f = 30.156 MSI

E_2^f = 2.86 MSI

G_{12}^f = 4.0 MSI

$\xi_e = 2$, $\xi_g = 1$

Also, $E_M = D_M^{-1}$ = 0.67 MSI From static tests at 75°F/50%R.H.

FIGURE 26 COMPLIANCE RELATIONSHIPS BETWEEN LAMINATES AND IN-SITU MATRIX

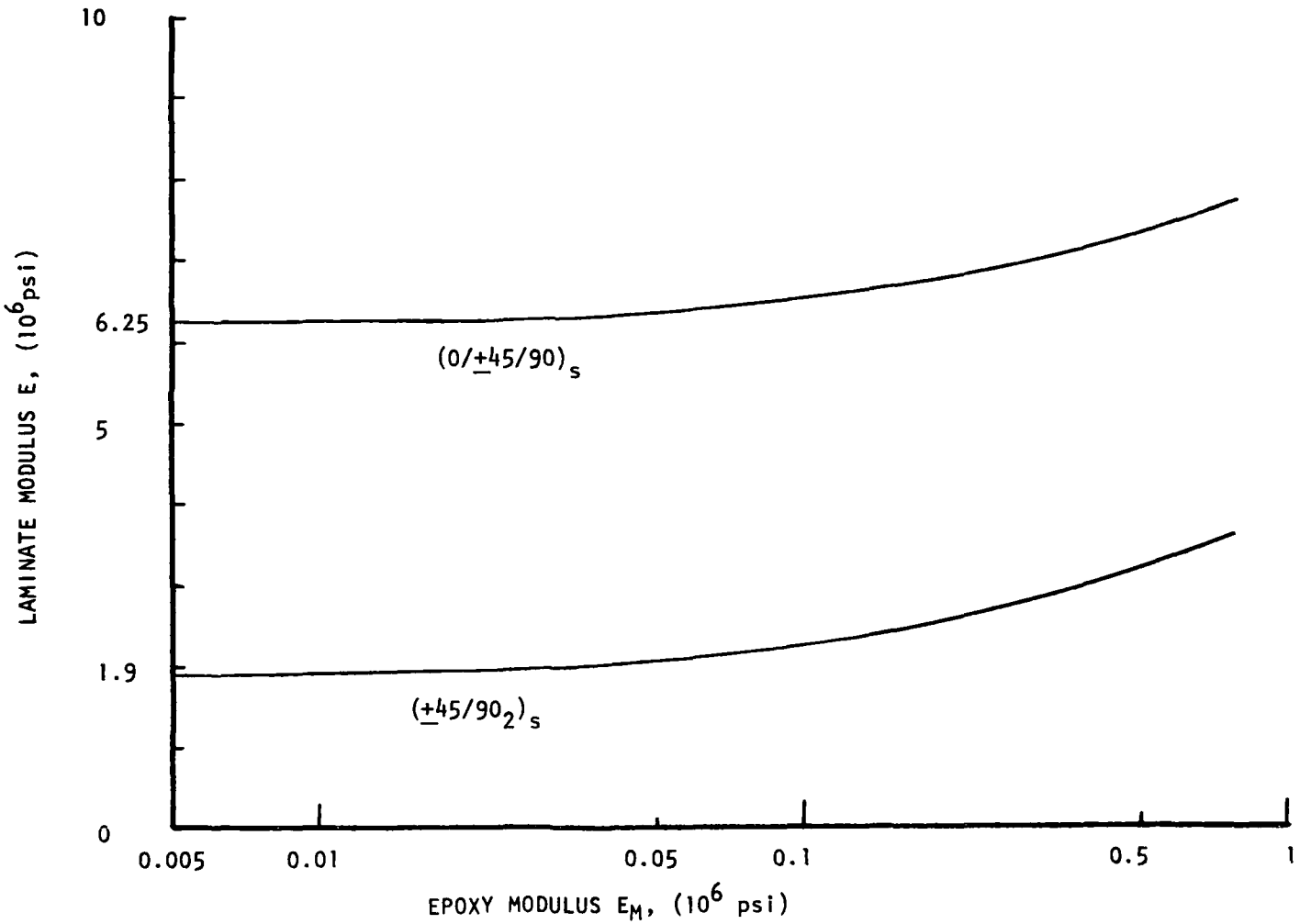

FIGURE 27 MODULUS RELATIONSHIPS BETWEEN LAMINATES AND THEIR IN-SITU MATRIX

in-plane strains through the laminate thickness; this uniformity is achieved through interlaminar shear and normal stresses, which in practice are limited to the neighborhood of the laminate edges unless the matrix modulus is extremely low compared to the fiber moduli.

As a working hypothesis for using these curves to interpret fatigue and static fracture data, we shall suppose that gross laminate failure initiates when microcracking and other degradation processes reduce the (effective) matrix modulus to a relatively very small value. (This same type of failure criterion was used successfully by Alexander et al.[8] in characterizing static fracture of a random glass fiber composite.) With this reduction, interlaminar stresses can be expected to produce overall sample failure through delamination and other complex fracture processes. Inasmuch as this latter stage of the failure process will be specimen size related, and therefore is not a fundamental characteristic of the laminate, it is reasonable to define a failure criterion in terms of some reduced value of the matrix stiffness for which interlaminar stresses and/or delaminations are widespread in the samples. This degraded matrix stiffness value may be somewhat laminate-dependent and possibly better characterized using orthotropic matrix moduli, but for now we shall arbitrarily interpret failure using the limiting laminate moduli for $E_M = 0$ in order to make a preliminary assessment of the failure model.

The horizontal lines drawn in Figures 10-13 and in Figures 19-20 represent the strain level where the S-N curve shows strong run up. The predicted mean strains using the laminate moduli for $E_M = 0$ are also indicated in the Figures. It is seen that the proposed criterion predicts more or less the strain at which the actual mean fatigue strain starts to increase rapidly with the number of cycles, and therefore represents a

conservative (but not too conservative) prediction of fatigue failure. With other R-values, total strain or other combinations of mean strain and strain amplitude may be a better failure parameter than mean strain; but additional study of this is needed.

As a further test of the failure criterion, static stress and strain at failure for the same laminates are plotted in Figure 28. Failure in the $(\pm 45/90_2)_s$ laminate is assumed to occur at the second slope change point in Figure 6; beyond this point the stress-strain curve is very flat, presumably corresponding to massive specimen damage as a result of widespread interlaminar stresses. Prediction of the failure secant modulus for both laminates, $(\pm 45/90_2)$ and $(0/\pm 45/90)_s$ is shown in Figure 28 using moduli from Figure 27 for $E_M = 0$. Good agreement with the experimental data is exhibited; since we have used $E_M = 0$, it is encouraging that the predictions are at the lower edge of most of the data.

The modulus of the $(\pm 45)_{2s}$ laminates vanishes when $E_M = 0$. However, as shown in Figure 29 (from data in Reference 2), the stress and strain values for static fracture fall reasonably close to the line predicted by using a laminate modulus corresponding to a matrix modulus which is 10% of that for the undamaged state. It should be added that if we had used this same matrix modulus in predicting static and mean fatigue moduli at failure for $(\pm 45/90_2)_s$ and $(0/\pm 45/90)_s$ laminates, the results would have been practically the same as for $E_M = 0$; i.e. for these laminates, there is little difference in the laminate moduli using either $E_M = 0$ or a 90% reduction factor applied to the undamaged value.

It is believed the above comparisons serve to bring out the importance of the behavior of the effective matrix modulus in understanding and predicting failure of composite materials. For example, various predictions, such as the effect of temperature and moisture on composite material failure,

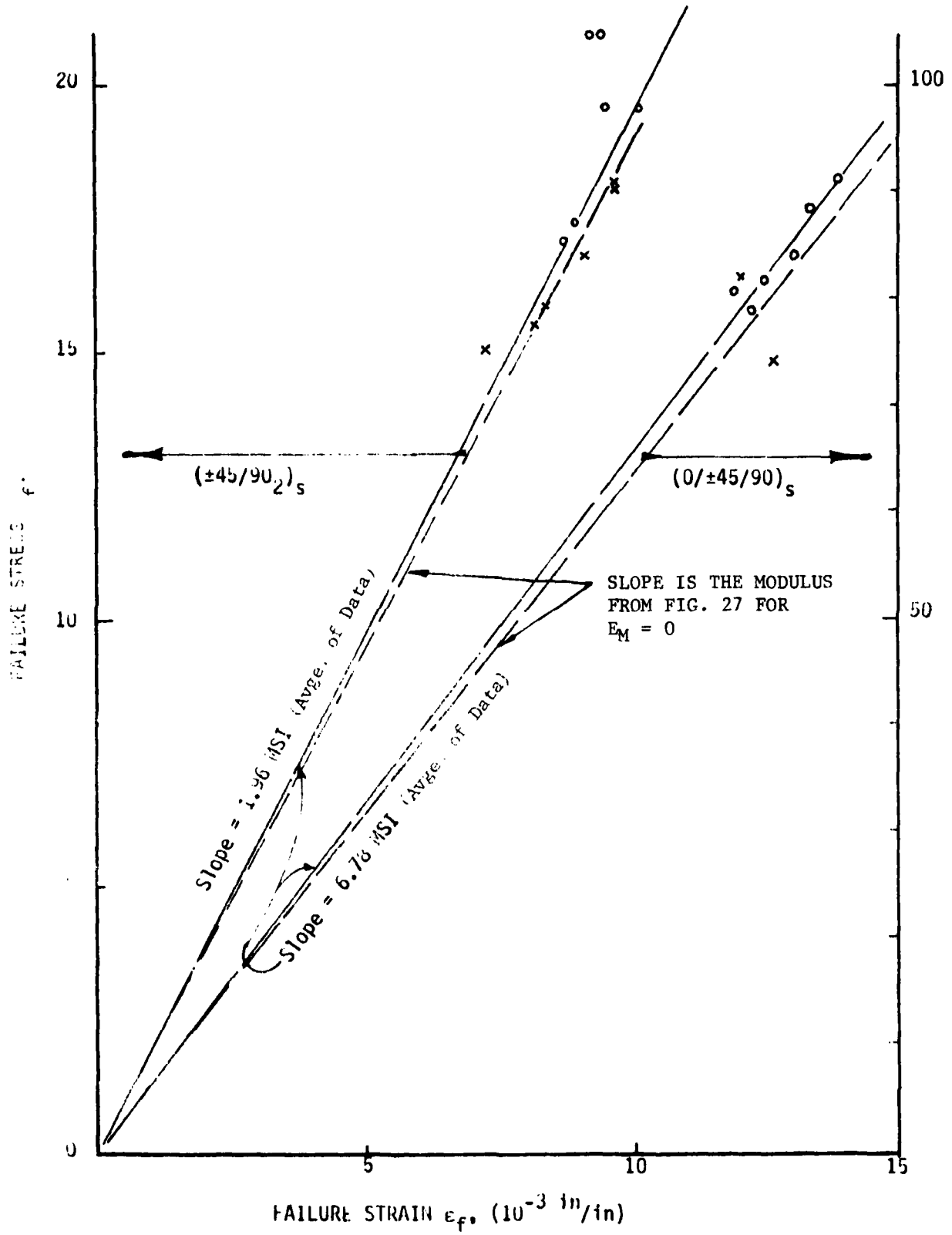

FIGURE 28. STATIC FAILURE ENVELOPE FOR $(0/\pm 45/90)_s$ AND $(\pm 45/90_2)_s$ SPECIMENS

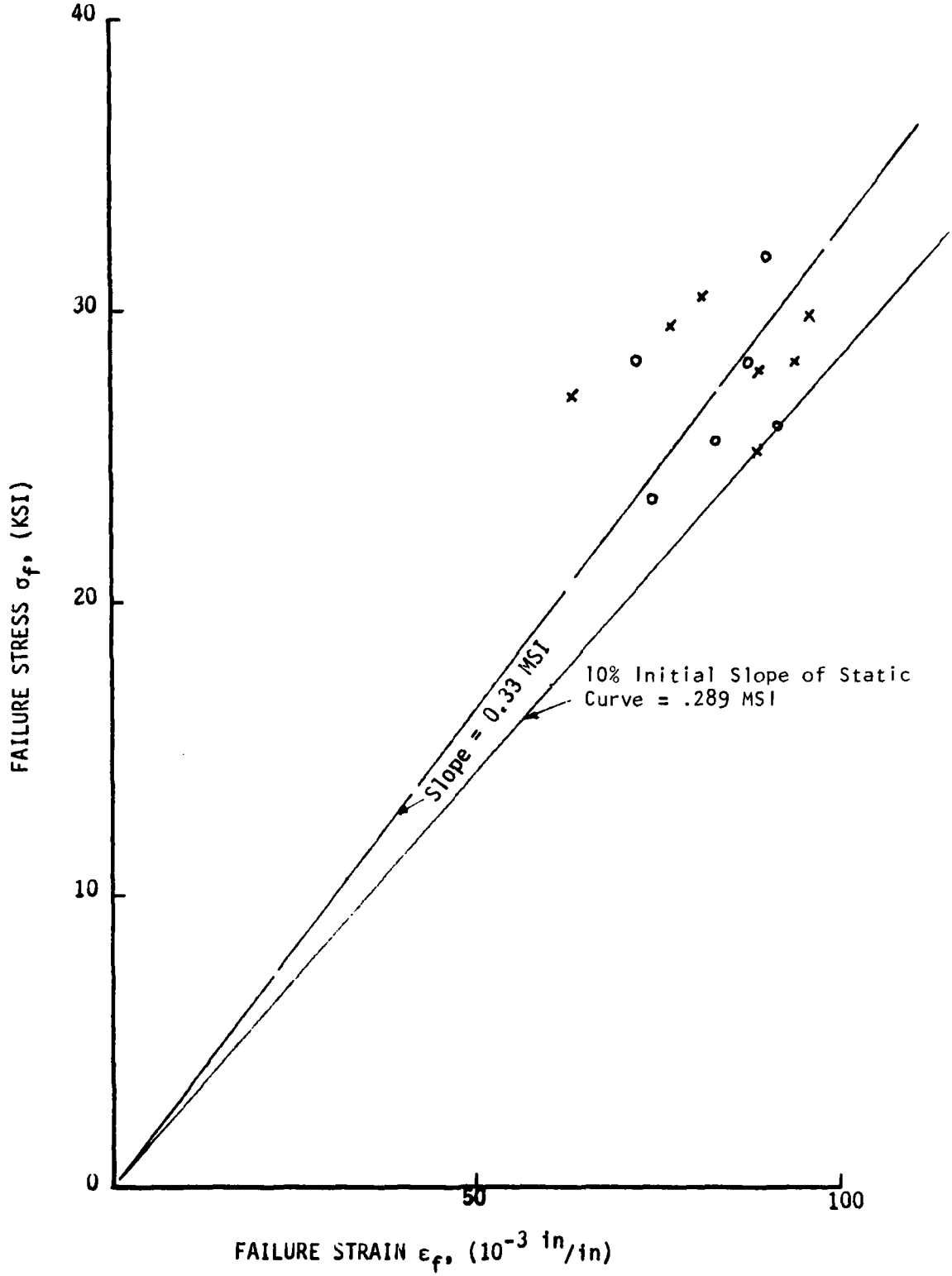

FIGURE 29. STATIC FAILURE ENVELOPE FOR $(\pm 45)_{2s}$ SPECIMENS

number of fatigue cycles-to-failure, creep-rupture times, etc., should be in large part concerned with prediction of effective matrix modulus. For example, it may be possible to predict the number of fatigue cycles to failure, by predicting average matrix softening within each ply in terms of the damage parameter,

$$\left[\int_0^{\xi} f(\sigma_{ef})^q d\xi_f\right] = \text{measure of matrix damage} \tag{1}$$

(where q is a positive constant and ξ_f is reduced time or reduced number of cycles) which results from the consideration of microcrack growth.[9,10] The quantity σ_{ef} is a suitably defined average stress invariant in the matrix, such as the average octahedral shear stress previously used to characterize nonlinear viscoelastic behavior of lamina.[11] The reduced time, ξ_f, is

$$\xi_f = \int_0^t dt \,/a'_{TM} \tag{2}$$

where a'_{TM} is not necessarily the same as a_{TH} for creep behavior at low stresses. Indeed, a'_{TM} can be expected to depend on not only temperature and moisture, but also on matrix stress level[11] (including residual stress); the differences between shift factors for each laminate studied in this program[1,2] may be due in part, at least, to the different matrix stress levels.

The most appropriate damage parameter(s) may depend to some extent on the moisture content, temperature, frequency, etc., considering the fact that these factors influence the nature of microcrack growth (i.e., continuous or stop-start (unstable) growth) as well as whether or not the matrix behaves in a brittle or ductile manner.[12-13] Nevertheless, it is suggested that a good starting point for predicting matrix degradation would be to use the damage parameter in Eq. (1) to evaluate the fatigue data collected in this research program. A test of the theory would consist of determining how well the criterion,

$$\int_0^{t_f} (\sigma_{ef})^q d\xi_f = \text{constant} \tag{3}$$

predicts failure time or number of cycles to failure for the critical ply; σ_{e_f}, as noted above, is possibly the average octahedral shear stress in the matrix and the critical ply for the laminates in Figure 27 would be assumed as 90^o ply. The particular laminate construction would determine the relation between σ_{e_f} and applied laminate stress, as well as the limiting laminate moduli for small values of E_M.

It should be noted that this approach to predicting failure of laminates is similar to that discussed by Halpin et al.[14] only to the extent that damage is assumed to depend on the history of stress raised to a power. In contrast to the theory in Reference 14, a measure of the matrix stress level, rather than externally applied stress, is used in the failure prediction.

In this discussion of failure theory, we have not introduced direct effects of delamination. Rather, delamination was tacitly assumed to occur (if significant at all) close to the time of failure, and to not have an important influence on the total time for progressive matrix damage. Nevertheless, the failure criterion, Eq. (3), could be viewed possibly as the measure of critical matrix softening for which the delamination energy release rate exceeds the surface energy required for delamination.

This aspect of the problem is under study as part of a separate project in recently begun analytical research at Texas A&M University under the direction of R. A. Schapery. Initially, the $(\pm 45/90_2)_s$ laminate is being studied; results for the critical matrix modulus and laminate failure strain will be compared with the data in this report. Further related work at Vought and Texas A&M University will be coordinated, and include consideration of direct coupling between progressive matrix softening and delamination. It is expected that an important result of these efforts will consist of a prediction of the influence of temperature and moisture on fatigue strength

(ref. Figures 18, 23, 24, 25) in terms of the in-situ matrix creep compliance and its dependence on temperature and moisture.

6.0 DISCUSSIONS AND CONCLUSIONS

Efforts in Phase II and Phase III of this program have generated most of the basic data believed needed for the characterization of the static fracture and fatigue failure AS/3501-6 graphite/epoxy material. Analysis of the data indicates that there is close correlation between the static fracture and the fatigue failure process through the matrix modulus, and two parts of the failure process can be hypothesized for composite specimens. First, microcracking and other degradation processes reduce the matrix (effective) modulus to a relatively small value. Second, due to the low matrix modulus, the interlaminar stress spreads out from the edge area. The zone of high interlaminar stress then initiates gross failure, possibly in the form of delamination.

The above assessment on the composite failure mechanism suggests that a failure can be predicted using a critical value for matrix modulus if one can neglect the time required for the stage of gross spreading of delamination of interlaminar stresses. Thus, prediction of the effective matrix modulus as a function of temperature, moisture, number of fatigue cycles, etc., is needed. For further development of the fatigue theory, it is important to test the fatigue failure criterion, equation (3), to predict number of cycles to failure by incorporating the limiting laminate moduli concept. Specifically, for further development work in fatigue characterization, we need to:

(1) Study in more detail the correlation between static fracture and fatigue failure from existing data.

(2) Perform calculations of the damage parameter, equation (3), for each ply and relate it to the effective modulus using strain data and predictions of laminate moduli.

(3) Characterize the shift factor a'_{TM} in fatigue as a function of temperature, humidity and matrix stress level.

(4) Determine through comparison of theory and experimental data the appropriate stress invariant in equation (3); existing static deformation and failure properties would provide data for initial comparison

These are the tasks to be conducted in Phase IV.

REFERENCES

1. Renton, W. J. and Ho, T., "The Effect of Environment on the Mechanical Behavior of AS/3501-6 Graphite/Epoxy Material", Final Phase I Report, NASC Contract No. N00019-77-C-0369, June 1978.
2. Ho, T., "The Effect of Environment on the Mechanical Behavior of AS/3501-6 Graphite/Epoxy Material, Phase II", ATC Report No. R-92100/9CR-61, Contract No. N00019-78-C-0599, Jan. 10, 1980.
3. Ho, T., "The Effect of Environment on the Mechanical Behavior of Kevlar/5208 Material", AMMRC Contract DAAG46-80-Q-0239.
4. Wang, A.S.D. and Crossman, F. W., "Some New Results on Edge Effect in Symmetric Composite Laminates", J. Composite Material, Vol. 11, 1977.
5. Pipes, R. B. and Pagano, N. J., "Interlaminar Stresses in Composite Laminates - An Approximate Elasticity Solution", J. of Applied Mechanics, September, 1974.
6. Pagano, N. J. and Pipes, R. B., "Some Observations on the Interlaminar Strength of Composite Laminates", Int. J. of Mechanical Science, Vol. 51, 1973.
7. Ramani, R. V. and Williams, D. P., "Notched and Unnotched Fatigue Behavior of Angle-Ply Graphite/Epoxy Composites", ASTM STP 636, Fatigue of Filamentary Composite Materials, 1977.
8. Alexander, R. M.,Schapery, R. A., Jerina, K. L., and Sanders, B. A., "Fracture Characterization of a Random Fiber Composite Material", Texas A&M University Report No. MM3979-80-4, April 1980. (To be published in ASTM Special Technical Publication, 1981)
9. Schapery, R.A., "A Nonlinear Constitutive Theory for Particulate Composites Based on Viscoelastic Fracture Mechanics", Proc. of JANNAF Structures & Mechanical Behavior Working Group, 12th. Meeting, Jan. 1974, CPIA Publication No. 253.

10. Schapery, R.A., "Nonlinear Fracture Analysis of Viscoelastic Composite Materials Based on a Generalized J-Integral Theory", Proceeding of Japan-U.S. Conference on Composite Mechanics: Mechanical Properties and Fabrication, January, 1981, Tokyo.

11. Lou, Y. C. and Schapery, R. A., "Viscoelastic Characterization of a Nonlinear Fiber-Reinforced Plastic", J. Composite Materials, Vol. 5, pp. 208-234, 1971.

12. Corten, H. T., "Fracture Mechanics of Composites," In Fracture, Vol. VII, H. L. Liebowitz, Editor, Academic Press, pp 675-769, 1972.

13. Yamini, S. and Young, R. J., "Stability of Crack Propagation in Epoxy Resins," Polymer, Vol. 18, pp 1075-1080, 1977.

14. Halpin, J. C., Jerina, K. L., and Johnson, T. A., "Characterization of Composites for the Purpose of Reliability Evaluation, "Analysis of Test Methods for High Modulus Fibers and Composites, ASTM STP 521, pp 5-64, 1973.

DISTRIBUTION LIST

	No. of Copies
Naval Air Systems Command Attn: Code AIR-5163D3 Washington, DC 20361	8
Office of Naval Research (Code 472) Washington, DC 20350	1
Office of Naval Research, Boston 495 Summer St. Boston, MA 02210 ATTN: Dr. L. H. Peebles	1
Naval Research Laboratory Codes 6306 and 6120 Washington, DC 20350	2
Naval Surface Weapons Center Code R-31 White Oak, Silver Spring, MD 20910	1
Naval Air Propulsion Test Center ATTN: J. Glatz Trenton, NJ 08628	1
Commander U. S. Naval Weapons Center China Lake, CA 92555	1
Naval Ship R&D Center ATTN: Mr. M. Krenzke, Code 727 Washington, DC	1
Naval Sea Systems Command Navy Dept. Codes 05R and 05D23 Washington, DC 20360	2
Commander Naval Air Development Center ATTN: Aero Materials Lab Aero Structures Div Radomes Section Warminster, PA 18974	3

DISTRIBUTION LIST (Cont'd)

	No. of Copies
Air Force Materials Laboratory ATTN: Codes LC (1 copy) LN (" ") LTF (" ") LAE (" ") Wright-Patterson AFB, OH 45433	4
Air Force Flight Dynamics Laboratory ATTN: Code FDTC Wright Patterson AFB, OH 45433	1
U. S. Applied Technology Laboratory U. S. Army Development Laboratories (AVRADCOM) ATTN: DAVDL-ATL-ATS Fort Eustis, VA 23604	1
Director Plastics Technical Evaluation Center Picatinny Arsenal Dover, NJ 07801	1
Department of the Army Army Materials & Mechanics Research Center Watertown, MA 02172	1
NASA Langley Research Center Hampton, VA	1
NASA Headquarters Code RV 2 (Mr. N. Mayer) 600 Independence Ave., SW Washington, DC 20546	1
AVCO Corporation Applied Technology Division Lowell, MA 01851	1
Bell Aerospace Co. ATTN: Mr. F. M. Anthony Buffalo, NY 14240	1
The Boeing Company Aerospace Division P. O. Box 3707 Seattle, WA 98124	1
Boeing Vertol Co. P. O. Box 16858 ATTN: Dept 1951 Philadelphia, PA 19142	1

DISTRIBUTION LIST (Cont'd)

	No. of Copies
Brunswick Corporation Technical Products Division 325 Brunswick Lane Marion, VA 24354	1
Celanese Research Company Box 1000 ATTN: Mr. R. J. Leal Summit, NJ 07901	1
Defense Ceramic Information Center Battelle Memorial Institute 505 King Ave Columbus, OH 43201	1
E. I. DuPont de Nemours & Co. Textile Fibers Dept. Wilmington, DE 19898	1
Ewald Associates, Inc. 105 Skyline Drive Morristown, NJ 07960	1
Fiber Materials, Inc. ATTN: Mr. J. Herrick Biddeford Industrial Park Biddeford, ME	1
General Dynamics Convair Aerospace Division ATTN: Tech Library P. O. Box 748 Fort Worth, TX 76101	1
General Dynamics Convair Division ATTN: Mr. W. Scheck; Dept. 572-10 P. O. Box 1128 San Diego, CA 92138	1
General Electric R&D Center ATTN: Mr. W. Hillig Box 8 Schnectady, NY 12301	1
General Electric Company Valley Forge Space Center Philadelphia, PA 19101	1

DISTRIBUTION LIST (Cont'd)

	No. of Copies
B. F. Goodrich Aerospace & Defense Products 500 South Main St Akron, OH 44318	1
Graftex Division EXXON Industries 2917 Highwoods Blvd. Raleigh, NC 27604	1
Great Lakes Research Corporation P. O. Box 1031 Elizabethton, TN	1
Grumman Aerospace Corp ATTN: Mr. G. Lubin Bethpage, LI, NY 11714	
Hercules Incorporated ATTN: Mr. E. G. Crossland Magua, UT 84044	1
HITCO 1600 W. 135th St Gardena, VA 90406	1
Illinois Institute of Technology Research Center ATTN: Dr. K. Hofer 10 West 35th St. Chicago, IL 60616	1
Lockheed California Co. ATTN: Mr. J. H. Wooley Box 551 Burbank, CA 91520	1
Lockheed-Georgia Co. ATTN: Mr. L. E. Meade Marietta, GA 30063	1
Lockheed Missiles & Space Co. ATTN: Mr. H. H. Armstrong, Dept. 62-60 Sunnyvale, CA 94088	1
Material Sciences Corporation 1777 Walton Road Blue Bell, PA 19422	1

DISTRIBUTION LIST (Cont'd)

	No. of Copies
McDonnell Douglas Corp. McDonnell Aircraft Co. ATTN: Mr. J. Juergens P. O. Box 516 St. Louis, MO 63166	1
McDonnell-Douglas Corp. Douglas Aircraft Co. ATTN: Mr. R. J. Palmer 3855 Lakewood Blvd. Long Beach, CA 90801	1
Monsanto Research Corp. 1515 Nicholas Road Dayton, OH 45407	1
North American Aviation Columbus Division 4300 E. Fifth Ave Columbos, OH 43216	1
Northrop Corp. 3901 W. Broadway ATTN: Mr. G. Grimes, Mail Code 3852-82 Hawthorne, CA 90250	1
Philco-Ford Corp. Aeronutronic Division Ford Road Newport Beach, CA 92663	1
Rockwell International Corp. ATTN: Mr. C. R. Rousseau 12214 Lakewood Blvd Downey, CA 90241	1
Stanford Research Institute ATTN: Mr. M. Maximovich 333 Ravenswood Ave, Bldg 102B Marlo Park, CA 94025	1
TRW, Inc. Systems Group One Space Park, Bldg. 01; Rm 2171 Redondo Beach, CA 90278	1
TRW, Inc. 23555 Euclid Ave Cleveland, OH 44117	1

DISTRIBUTION LIST (Cont'd)

	No. of Copies
Union Carbide Corporation Chemicals & Plastics One River Road Bound Brook, NJ	1
Union Carbide Corporation Carbon Products Division P. O. Box 6116 Cleveland, OH 44101	1
United Aircraft Corporation United Aircraft Research Laboratories E. Hartford, CT 06108	1
United Aircraft Corporation Pratt & Whitney Aircraft Division East Hartford, CT 06108	1
United Aircraft Corporation Hamilton-Standard Division ATTN: Mr. T. Zajac Windsor Locks, CT	1
United Aircraft Corporation Sikorsky Aircraft Division ATTN: Mr. J. Ray Stratford, CT 06602	1
University of California Lawrence Livermore Laboratory ATTN Mr. T. T. Chiao P. O Box 808 Livermore, CA 94550	1
University of Maryland ATTN. Dr. W. J. Bailey College Park, MD 20742	1
University of Wyoming Mechanical Engineering Dept. ATTN Dr D. F. Adams Laramie, WY 82071	1
Westinghouse R&D Center ATTN Mr Z. Sanjana 1310 Beulah Road Churchill Boro Pittsburgh PA 15235	1

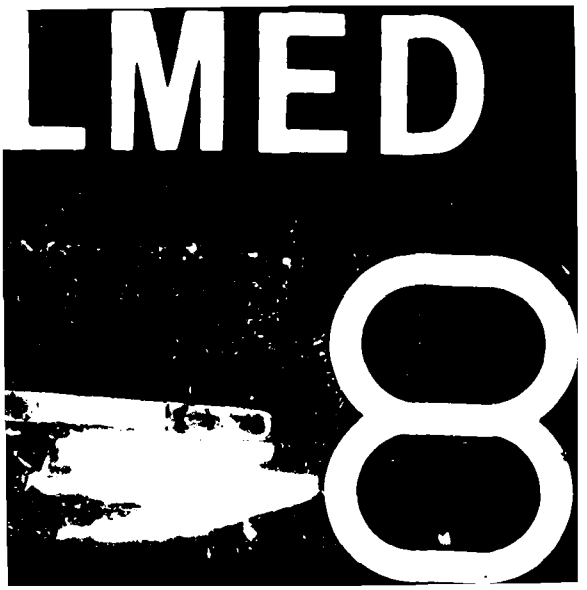
LMED
8